catalysts

MDPI

Review

Two-Dimensional Materials and Composites as Potential Water Splitting Photocatalysts: A Review

Zubia Saleem, Erum Pervaiz *, M. Usman Yousaf and M. Bilal Khan Niazi

Department of Chemical Engineering, School of Chemical & Materials Engineering (SCME), National University of Sciences & Technology (NUST), Sector H-12 Islamabad, Islamabad 44000, Pakistan; zubia.saleem92@gmail.com (Z.S.); usman.yousaf93@gmail.com (M.U.Y.); m.b.k.niazi@scme.nust.edu.pk (M.B.K.N.)

* Correspondence: erum.pervaiz@scme.nust.edu.pk; Tel.: +92-51-9085-5113

Received: 28 November 2019; Accepted: 18 January 2020; Published: 24 April 2020

Abstract: Hydrogen production via water dissociation under exposure to sunlight has emanated as an environmentally friendly, highly productive and expedient process to overcome the energy production and consumption gap, while evading the challenges of fossil fuel depletion and ecological contamination. Various classes of materials are being explored as viable photocatalysts to achieve this purpose, among which, the two-dimensional materials have emerged as prominent candidates, having the intrinsic advantages of visible light sensitivity; structural and chemical tuneability; extensively exposed surface area; and flexibility to form composites and heterostructures. In an abridged manner, the common types of 2D photocatalysts, their position as potential contenders in photocatalytic processes, their derivatives and their modifications are described herein, as it all applies to achieving the coveted chemical and physical properties by fine-tuning the synthesis techniques, precursor ingredients and nano-structural alterations.

Keywords: water splitting; photocatalyst; graphene oxide; phosphorene; graphitic carbon nitride; MOFs

1. Introduction

Today, energy is one of the utmost critical environmental, economic and political issues due to the contributing factors of continuously increasing global population, escalating urbanization and growing energy consumption. These dynamics are compelling researchers and front-runners in political, social, environmental and industrial fields towards a shift from conventional energy production methods towards more innovative, sustainable, efficient, safe and environmentally benign technologies and materials. The total energy consumption of the entire globe is 18.5 TW per year currently, which is expected to rise to 40.8 TW by 2050 [1]. Approximately 85% of total energy usage comes from fossil fuel. It is estimated that there are sufficient fossil fuel resources to meet global energy demands for several centuries [2]. However, irreversible climate change due to generation of greenhouse gases, depletion of fossil fuel reserves, geopolitical conflicts and other environmental concerns are continuous threats for secure and sustainable energy supply. Therefore, the world needs to devise advanced, sustainable methods and sources competitive to fossil fuels in terms of efficiency and economics while ensuring minimal environmental damage [3]. The sun is an everlasting source of inexhaustible energy with which to produce hydrogen, which proves to be potential candidate to meet secure energy demands due to environmental friendliness, high energy value and the possibility of onsite production [4]. The amount of solar energy reaching earth is around 9.5×10^{16} J/s; that is 10^4 times the total usage by entire human population, endorsing its candidature for potential sustainable energy sources [5]. The major research concern for harnessing solar energy is the production of solar fuel. Conventional technologies of solar energy production suffer from many downsides, such as the limited

storage capacity for the energy, the intermittent availability in certain areas and the economic feasibility of the process. The steam reforming process is traditionally used for hydrogen production from fossil fuels, which is not considered as sustainable in the long haul due to massive carbon dioxide emission and depleting resource trends. Catalytic steam reforming using fossil fuels is virtually the only industrial process responsible for producing the entire hydrogen supply of the world today, with electrolysis contributing only a meager 4% via water electrolysis. There is a growing interest in generating hydrogen from sustainable and renewable resources using environmentally friendly methods to deliver inexpensive and clean energy [6]. Photocatalytic water splitting activity is one of the key research areas for onsite hydrogen production and storage [7–16]. It is one of the emerging process for harnessing solar energy into fuel in the form of hydrogen without any use of fossil fuels or emission of carbon dioxide. There is a growing interest in the field of semiconductor photocatalysis [17] which could be used for water dissociation into constituent oxygen and hydrogen gases using solar energy, which is abundantly available all over the world. Solar energy conversion in the form of hydrogen via photocatalytic water splitting has become an attractive subject [18].

The prerequisites to an energy efficient, cost effective and operationally feasible photocatalyst are the ability to effectively harvest and utilize photons in the visible light region to generate electron-hole pairs; lower band gap energies; unimpeded mobility of charge carriers; a low recombination rate of electron-hole pairs; and a greater surface area, resulting in a higher number of exposed active sites. The earliest discoveries fulfilling these requirements comprised granular semi-conducting materials and their derivatives, such as ZnO and TiO_2 [19]. But these conventional photocatalysts have several shortcomings, such as:

(1) Their higher band gap energy, making the materials suitable for mainly UV light absorption instead of visible light [20];
(2) Only having the ability to catalyze either water oxidation or reduction at a time, leading to their unsuitability to act as dual function overall water splitting catalysts [21];
(3) Their higher charge recombination rates in bulk medium and on the surface, resulting in lower activity [22];
(4) Inaccessibility of active sites lying in bulk material [23].

Further research and development in this regard led to the conclusion that the nano-materials are better photocatalysts because of their high surface area property [24,25]. Among nanomaterials, 2D materials are promising photocatalyst alternatives due to their sheet-like structures; electrical, thermal and mechanical properties; the operational advantages of being easily handleable; having the ability to form integrated composites with highly photoactive co-catalysts; and having higher surface to volume ratios. The bi-layer and mono-layer 2D nanocrystals and nanosheets provide the basis for highly exposed active sites and faster charge transfer schemes [26], while the doped precious and photo-active metals and their related compounds offer the added compensation of higher light absorption capacity and lower band gap energy [27,28].

1.1. Photocatalysis: Theoretical Digest

Hydrogen production by photocatalytic water splitting has proven to be a superlative solution for resource and economics related problems in novel hydrogen production methods. The process is centered on a semiconducting catalyst material and sunlight to convert the light energy to chemical energy, also termed "artificial photosynthesis." The photons of light having higher energy than the energy gap of semiconducting material, when irradiated on the photocatalyst material, results in photo generated charge carriers usually termed the electron hole pair. This generation of electron-hole pairs in the conduction band and valence band acts as the foundation for redox reactions, as indicated below [29,30]:

Overall:

$$2H_2O\ (l) \xrightarrow{Photon\ energy>1.23\ eV} O_2(g) + 2H_2\ (g)$$

$$E^o = 1.23\ V.$$

The oxidation and reduction half reactions at anode and cathode, respectively, under acidic (low pH) solutions proceed as:

Oxidation:

$$2H_2O\ (l) + 4h^+ \rightarrow O_2(g) + 4H^+(aq)$$

$$E^o_{oxidation} = -1.23\ V.$$

Reduction:

$$2H^+ + 2e^- \rightarrow O_2(g) + 2H_2\ (g)$$

$$E^o_{reduction} = 0\ V.$$

Under basic (high pH) conditions, the chemical reactions are represented as:

Oxidation:

$$2OH^-(aq) \rightarrow \frac{1}{2}\ O_2(g) + H_2O\ (l) + 2e^-\ .$$

Reduction:

$$2H_2O\ (l) + 2e^- \rightarrow H_2\ (g) + 2OH^-.$$

The holes generated in the valence band resultantly are responsible for oxidation of adsorbed species (water in this case) releasing oxygen, and the agitated electrons from the conduction band are the reducing agents to produce hydrogen from in-contact water molecules as shown in Figure 1.

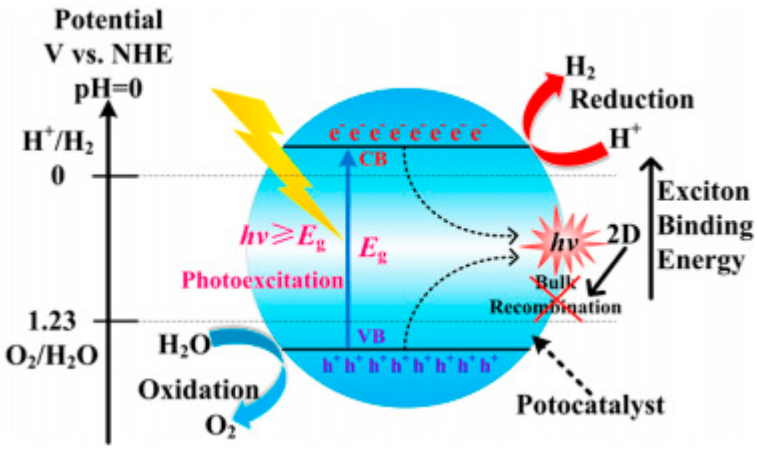

Figure 1. Schematic illustration of basic processes in photocatalytic water splitting. (Reprinted with permission from ACS Catal. 2018, 8, 3, 2253–2276, Publication Date: 30 January 2018. Copyright (2018) American Chemical Society [23]).

The production of charge carriers, such as electron and hole ones, is a fundamental step for all photocatalytic processes; other crucial factors include the width of material band gap and the energy levels of both conduction and valence bands of the material. For a feasible reaction to occur, the conduction band of the electron acceptor species should be more positive than the conductive band of the semiconductor photocatalyst, whereas the valence band of the electron donor type must be more negative than the semiconductor's valence band, and the minimum band gap must be greater than 1.23 eV [31]. As a result of the interface electron transfer process, the redox reaction takes place and the photolysis of water molecules occur.

1.2. Limitations of Photocatalytic Water Splitting

1. To catalyze the splitting of water at the interface of electrolyte and electrode, the charge carriers are required to be transferred to catalyst surface once the electron-hole pairs are created. The quick

recombination of photo-generated electron-hole pairs (Figure 2) releasing heat or photon energy before they can catalyze the redox reactions is a major challenge in this step, requiring a high degree of crystallinity [32].

2. The predilection for semiconductor materials to work under the ultraviolet (UV) light is another major challenge, as only about 4% of solar energy is comprised of UV light. It is advantageous for photocatalysts to work under visible light, which requires the band gap to be in visible range.
3. Photo-corrosion and catalyst decay are also among the limitations of the photocatalytic splitting of water. TiO_2, ZrO_2, $KTaO_3$, $SrTiO_3$ and $BiVO_4$ are among the notable contenders for photocatalytic water splitting because of having band gaps around 1.23 eV. Typical sulfide-based photocatalysts, such as cadmium sulfide (CdS), have a tendency to undergo decay under operating conditions due to oxidation of sulfide into elemental sulfur at the same potentials that are used for water splitting, requiring the use of certain sacrificial reagents, e.g., sodium sulfide, to control any sulfur lost [33].

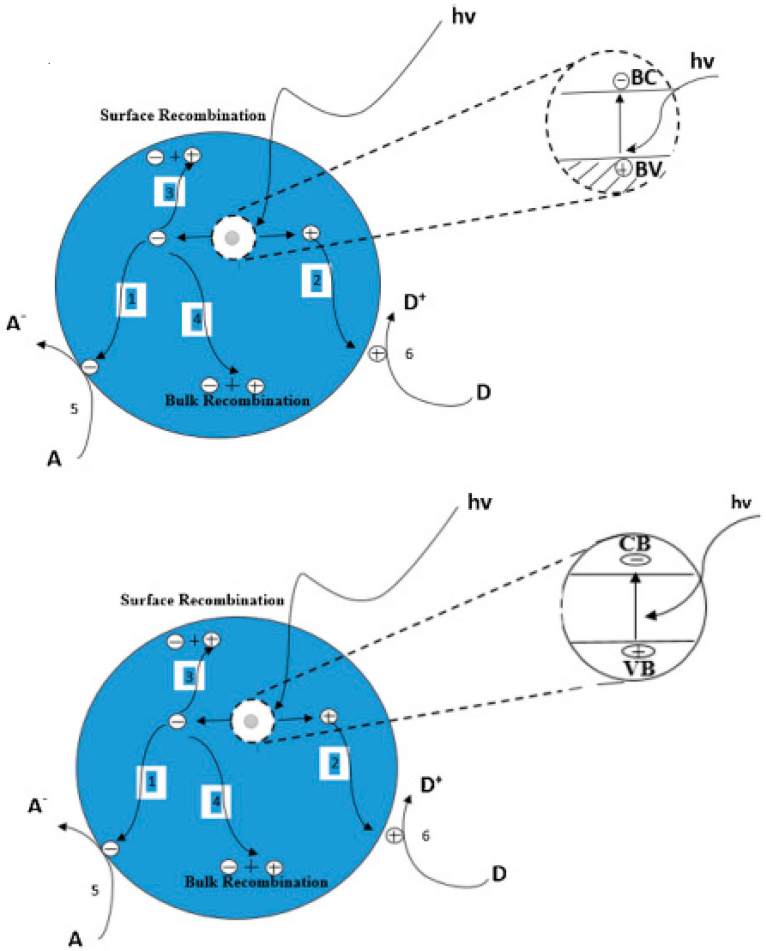

Figure 2. Schematic of charge carrier dynamics in a semiconductor: one electron transported to the surface; two holes transported to the surface; three surface recombinations; four bulk recombinations; five electron transfers to respective acceptor molecules; and six hole trappings by a donor molecule. (Reprinted with permission from [34]. Copyright (2019), Elsevier).

2. Two Dimensional Materials as Photocatalysts for Water Splitting

A good photocatalyst must possess the characteristics of photo-activity, thermal stability, photo-stability, chemical inertness, low cost, non-toxicity and post-reaction recoverability [35]. To tackle the environmental pollution factor, metal-free catalysts are always the first priority for synthesize with

maximum efficiency. The first and second generation of catalysts include combinations of inorganic materials [36] and various oxides and sulfides of metals, but the main problem of these materials is the toxic and corrosive nature [33,37]. Among various other photocatalyst materials available, 2D materials are promising candidates for the water splitting applications, because of merits, such as:

(1) The adjustable number of layers, so that the band gap and photo-absorption can be tuned [38].
(2) The sheet-like ultra-thin structure facilitating the charge transport towards surface, resulting in lower recombination rate [39].
(3) The enhanced specific surface area leading to greater exposure of active sites on surface and better catalytic performance [40].

The fundamental strategies to synthesizing 2D nanosheets comprise top-down and bottom-up methods, which vary on the basis of starting precursors and treatment methods also shown in Figure 3.

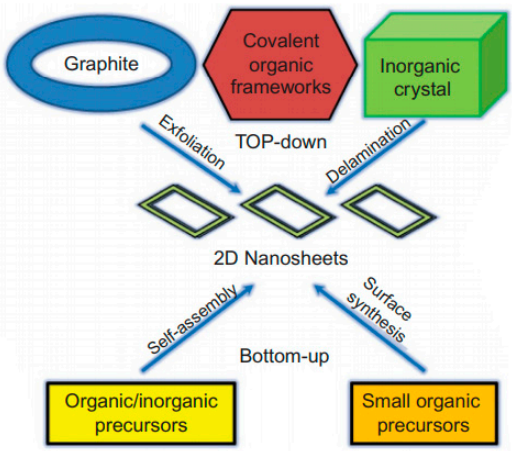

Figure 3. Schematic illustration of top-down and bottom-up strategies toward the synthesis of 2D nanosheets. (Reprinted with permission from [41]. Copyright (2015), Elsevier).

Till now, various 2D materials have been discovered by researchers, such as graphene, graphitic carbon nitride, black phosphorus/phosphorene and hexagonal boron nitride. All these materials have proven potential for water splitting activity by photocatalysis [42]. 2D materials show unusual structural, electronic and optical properties [43]. However, some limitations have been observed in terms of reaction completion due to the recombination rate of the electrons and holes which carry out reactions. In the search for alternatives to metal-based systems, metal-free elementals and compound photocatalysts have recently been developed. Red-P, alpha-sulfur and boron are notable examples reported in the literature [44]. However, these elemental photocatalysts exhibit low photocatalytic activity. There are various techniques that researchers employ to enhance activity majorly, including doping, sensitization, tuning morphology and making heterostructures with other materials [45]. The search for a non-toxic, inexpensive, corrosion resistant photocatalyst with a focus on the design and efficiency of photocatalyst, while assessing the activity for economical and scalable hydrogen generation, is ongoing. Table 1 summarizes the discussed literature in a comprehensive manner. The main focus of this paper is to go over 2D materials, their modifications and the different techniques that have been employed to enhance their photocatalytic water splitting performances. Said materials include, but are not limited to, graphitic carbon nitride, graphene, black phosphorus, metal phosphides and metal organic frameworks. Figure 4 presents the bandgap energies of all potential 2-D materials.

Table 1. A summary of recent studies on ultra-thin 2D photocatalysts. (Adapted with permission from [46], copyright (2017); Wiley and [47], copyright (2019); Nanotechnology, NCBI and [48], copyright (2019), Springer) (Unless otherwise specified).

Photocatalyst	Thickness (nm)	Bandgap (eV)	Sacrificial Agent	Co-Catalyst	Light Source	Type of Reaction	Activity (μmol/g·h)	Ref.
Pore rich WO_3 ultra-thin nanosheets	3.8	2.89, CB −0.40, VB 2.48	0.5 mol/L Na_2SO_4	-	300 W Xe lamp	OER	Photocurrent density 2.14 mA/cm^2 at 1.0 V	[49]
O-vacancy-rich In_2O_3 nanosheets	0.9	2.18	-	-	300 W Xe lamp with 420 nm cutoff filter	OER	Photocurrent density 1.73 mA/cm^2 at 0.576 V	[50]
Surface atomic SnS sheets	0.57	1.47	0.5 mol/L Na_2SO_4	-	300 W Xe lamp with 420 nm cutoff filter	Overall	Photocurrent density of 5.27 mA/cm^2 at 0.8 V	[51]
Single layer SnS_2	0.61	2.23	-	-	300 W Xe lamp with 420 nm cutoff filter	Overall	Photocurrent density of 2.75 mA/cm^2 at 1.0 V	[52]
ZnSe	0.85	3.5	0.5 mol/L Na_2SO_4	-	300 W Xe lamp	Overall	Photocurrent density of 2.14 mA/cm^2 at 0.72 V	[53]
Cu_2O	0.62	1.92	0.5 mol/L Na_2SO_4	-	300 W Xe lamp with 420 nm cutoff filter	HER	Photocurrent density of 3.98 mA/cm^2 at −1.0 V	
HNb_3O_8	1.3	3.68	10 vol% TEOA	1 wt% Pt	125 W Hg lamp	HER	≈610	[54]
$HNbWO_6$	1.8–2.0	3.13, CB −0.68, VB 2.45	TEOA	1 wt% Pt	300 W Xe lamp	HER	1986.25	[55]
$SnNb_2O_6$	≈3	2.43	20 vol% lactic acid	0.3 wt% Pt	300 W Xe lamp with 400 nm cutoff filter	HER	264	[9]
CoOOH	1.5	2.4	0.5 M Na_2SO_3	-	300 W Xe lamp	HER	1200	[56]
CdS	≈4	≈2.86	0.25 M Na_2S, 0.25 M Na_2SO_3	-	300 W Xe lamp with 420 nm cutoff filter	HER	41,100	[57]
O-doped $ZnIn_2S_4$	6	2.07, CB −1.34, VB 0.73	0.25 M Na_2SO_3, 0.35 M Na_2S	-	300 W Xe lamp with 420 nm cutoff filter	HER	2120	[58]
g-C_3N_4	≈2	2.97	10 vol% TEOA	6 wt% Pt	300 W Xe lamp	HER	170.5	[39]
g-C_3N_4	≈2	2.65	10 vol% TEOA	3 wt% Pt	300 W Xe lamp with 420 nm cutoff filter	HER	1860	[59]
$MoS_2/Bi_{12}O_{17}Cl_2$	0.71 of $Bi_{12}O_{17}C_{l2}$	≈2.5	0.3 M Ascorbic acid	-	300 W Xe lamp with 420 nm cutoff filter	HER	33,000	[60]
Rh-doped calcium niobate	≈2.8–3.0	≈1.9	10 vol% CH_3OH	Rh	500 W Xe lamp	HER	76,960	[61]
C-BN	3–4	2.72, CB −1.24, VB 1.48	10 vol% TEOA	1 wt% Pt	300 W Xe lamp	HER	≈920	[62]
Rh single atoms/TiO_2	0.7	-	20 vol% CH_3OH	Single atom Rh	500 W Xe lamp	HER	2550	[63]
$MoSe_2/ZnIn_2S_4$	2.5 of $ZnIn_2S_4$	≈2.75	10 vol% Lactic acid	1 wt% $MoSe_2$	300 W Xe lamp with 400 nm cutoff filter	HER	6454	[64]

Table 1. *Cont.*

Photocatalyst	Thickness (nm)	Bandgap (eV)	Sacrificial Agent	Co-Catalyst	Light Source	Type of Reaction	Activity (μmol/g·h)	Ref.
Ti_3C_2/g-C_3N_4	1.7–2.6 of Ti_3C_2	-	10 vol% TEOA	3 wt% Pt, 3 wt% Ti_3C_2	200 W Hg lamp λ > 400 nm	HER	72.3, 0.81% quantum efficiency at 400 nm	[65]
10% Fe_2O_3/g-C_3N_4 (1.0 wt% Pt)	21 Fe_2O_3	2.8 of g-C_3N_4, 2.1 of Fe2O3	15 vol% TEOA	1 wt% Pt	350 W xenon lamp λ > 420 nm	HER	398.0	[66]
WO_3/$ZnIn_2S_4$	-	2.4 of $ZnIn_2S_4$	0.25 M Na_2SO_3/0.35 M Na_2S	-	300 W xenon lamp λ > 420 nm	HER	2202.9	[67]
Cu_2S/$Zn_{0.67}Cd_{0.33}S$	5	2.28–2.5	0.1 M Na_2S/Na_2SO_3	Cu_2S	300 W xenon lamp λ > 420 nm	HER	15270, quantum efficiency 18.15% at 420 nm	[68]
15% WO_3/g-C_3N_4	2.5–3.5	2.77 of WO_3 and 2.68 of g-C_3N_4	20 vol% Lactic acid	2 wt% Pt	350 W xenon lamp	HER	982	[69]
25.0% UNiMOF/g-C_3N_4	3.04 UNiMOF	-	10 vol% TEOA	-	300 W xenon lamp λ > 420 nm	HER	400.6, quantum efficiency 0.979% at 420 nm	[70]
0.75% MoS_2/g-C_3N_4	8–10 of g-C_3N_4	-	0.1 M TEOA	0.75 wt% MoS_2	300 W xenon lamp λ > 420 nm	HER	1155, quantum efficiency 6.8% at 420 nm nm	[71]
MoS_2/$SnNb_2O_6$ (1.0 wt% Pt)	-	2.59 of SNO, 1.8 of MoS_2	20 vol% CH_3OH	1 wt% Pt	300 W xenon lamp λ > 420 nm	HER	258	[72]
$Bi_6Fe_2Ti_3O_{18}$/BiOBr ferroelectric heterostructure	20–50	2.5 of BFTO	0.2 g $AgNO_3$	-	300 W Xe arc lamp λ > 420 nm	OER	13.8	[73]
Ultrathin Bi_3O_4Cl/BiOCl	0.799–0.961	2.6	$AgNO_3$ and $FeCl_3$	-	300 W Xe lamp with the 400 nm cut-off filter	OER	58.6	[74]
$MoSe_2$/Ag_3PO_4 Heterojunction	-	-	0.5 mol/L Na2SO4	-	white LED	OER	182	[65]
BiO_{2-x} Ultra-thin nanosheet	5–10	1.3	Methyl viologen (2:20 ratio)	-	300 W Xenon arc lamp	OER	2715.443	[75]
CoO_x/hexagonal α-Fe_2O_3	-	2.09 of α-Fe_2O_3	0.1 g $AgNO_3$	5 wt% CoO_x	300 W Xenon lamp with λ 400 nm cut-off filter	OER	195.19	[76]
Co-$Zn_{0.5}Cd_{0.5}S$	-	2.45	Na_2S–Na_2SO_3	0.5 wt% Co	visible light (>420 nm)	HER	17.36	[77]
700-CoOx-C	-	-	$[Ru(bpy)_3]^{2+}$–$Na_2S_2O_8$	-	visible light (>420 nm)	OER	0.039	[78]

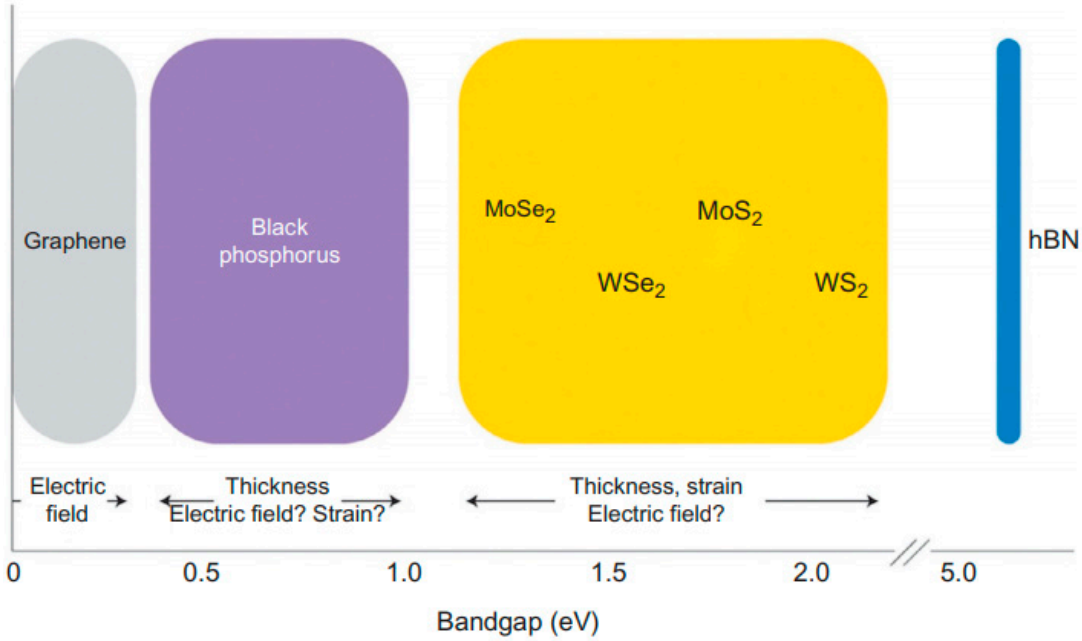

Figure 4. Bandgap energies of several layered materials used for nanoelectronics. (Reprinted with permission from [41]. Copyright (2015), Elsevier).

2.1. Graphitic Carbon Nitride and Derivatives

Graphitic carbon nitride is metal-free polymeric catalyst comprised of repeating triazine units. It is proving to be a highly efficient catalyst for photocatalytic activity with band gap of 2.56–2.70 eV. Due to highly efficient performance with an environmentally friendly nature, it is one of the most highly esteemed materials for water splitting. Due to some of its limitations, research is underway to make it more feasible and economical with improved activity. Different techniques, such as morphological alteration by changing temperature, modifying g-C_3N_4 with some metal and doping, for making heterostructures, have been investigated [79–81]. These modifications are targeted toward achieving a highly efficient catalyst by lowering the recombination rate of electrons and holes, improving value and improving environmental friendliness as much as possible [82]. 2D nanomaterials are being fabricated by facile and reliable methods: top-down ones include thermal exfoliation, chemical exfoliation, mechanical cleavage and selective etching; the bottom up approaches include chemical vapor deposition and wet synthesis methods. The most employed technique for the fabrication of 2D g-C_3N_4 is thermal treatment [83]. This facile method is easy to scale up for industrial level synthesis. However, in order to improve the photocatalytic performance, different techniques are employed and are under investigation to get maximum efficiency of a given material. Different temperature controlled synthesis techniques have been investigated to alter the morphology of the material [84]. Quan Gu investigated the morphological evolution of graphitic carbon nitride nanostructures and also evaluated their photocatalytic activities under visible light. The materials were synthesized at different temperatures, and showed different morphologies, optical properties, energy band structures and photocatalytic activity for water splitting. By changing the temperature, different structures, such as nanosheets, nanotubes and nanoparticles, were observed. BET surface area increased dramatically from 4.5 m^2/g of bulk g-C_3N_4 to 210.1 m^2/g of modified sample obtained at 540 °C. The exfoliated structures showed better activity for water splitting; i.e., 297 and 120 μmol/g·h for HER and OER respectively [85]. Zhi -An Lan modified g-C_3N_4 with bromine to investigate the change in properties. It was observed to get enhanced optical, conductive and photocatalytic properties of g-C_3N_4. The optimal catalyst CNU-Br 0.1 demonstrated more than two times higher H_2 evolution activity than pure CNU [86]. Junqing Yan fabricated g-C_3N_4/TiO_2 heterojunction by the hydrothermal method to get good production and separation of charge carriers. The fabricated TiO_2/g-C_3N_4 samples are active

in the hydrogen evolution reaction of water splitting with the best performance of 700 μmol/g·h and better photo-stability [87,88]. Recently, Yuhao Yang proposed a 2D/2D heterojunction strategy in order to compensate for low efficiency of charge separation in ultra-thin g-C_3N_4 2D sheets. The high surface area interface of g-C_3N_4 nanosheets and 2D TiO_2, coupled with favorable band structure, reliability of operation and stability of TiO_2 nanosheets resulted in high H_2 evolution rates and a robust, recyclable photocatalyst [89]. Guigang Zhang conducted some experimental studies of various redox cocatalysts, reporting g-C_3N_4 modified with Pt, PtO_x, and CoO_x. The results proved that cocatalysts, especially Pt/g-C_3N_4, show potential for water splitting activity without the use of a sacrificial agent [88]. Yaping Zeng fabricated $NiTiO_3$/g-C_3N_4 heterostructured material by the sol gel method. It was observed that $NiTiO_3$ had a suitable band gap and unique photo response in visible light range. It showed three times the activity of $NiTiO_3$/g-C_3N_4 hybrid catalysts, as compared to pure g-C_3N_4 and 3 wt%, the catalysts presented optimal activity. This is ascribed to the strong light absorption in the visible region and the prolonged recombination rate of electrons and holes [90].

Xiaojie She aimed at the template free synthesis of porous ultrathin nonmetal doped g-C_3N_4 nanosheets for increased H_2 production. The formation of an ultrathin structure and the introduction of oxygen proved favorable for the enhancement of the photocatalytic performance. The average H_2 evolution rate of came out at ≈ 3786 μmol/g·h; that is five times that of bulk g-C_3N_4 photocatalyst material. This increased activity was endorsed due to more adsorption and active sites, the enhanced redox ability and improved electron transportability due to the introduction of the electrophilic groups (C-O, C=O and COOH) [91]. Mohammad W. Kadia et al., in their work, claimed to increase the efficiency of water splitting using visible light, and also increased the charge separation using mesoporous g-C_3N_4 which was coated over by WO_3. They further claim that by coating a semiconductor surface with a metal-oxide, it can capture the surface electrons, and hence can increase the charge separation. The parameters affected the WO_3/g-C_3N_4 in charge separation ability, mesoporous structure gap between valence and conduction band high surface area [92]. Recently, a step-heterojunction scheme was demonstrated by Junwei, Fu. et al. [69], whereby 2D/2D WO_3/g-C_3N_4 photocatalyst was developed by ultrasonic exfoliation of WO_3 and dual-step thermal etching of g-C_3N_4 in bulk forms. The resulting material showed 1.7 times higher H_2 production activity by barricading the charge recombination. This advancement is owed to the fact that the electronic transfer on interface of both materials from g-C_3N_4 to WO_3 balanced the higher fermi level of g-C_3N_4 and the lower fermi level of WO_3. This mechanism creates a continuous electron transfer trend and simultaneously prevents the useful charge carriers (electrons from CB of g-C_3N_4 and holes from VB of WO_3) from recombining. $KNbO_3$ has been researched extensively in terms of photocatalytic activity for water splitting, but it has low quantum efficiency, showing water splitting activity only under UV light irradiation. It has been used to enhance g-C_3N_4 activity by making heterojunction. Dongbo, Xu. et al., in their research, presented the synthesis of g-C_3N_4/$KNbO_3$ heterojunction composites by the hydrothermal method and used them for water splitting and hydrogen production using sunlight. The g-C_3N_4 and $KNbO_3$ had better performances for water splitting by more than two and 1.8 times that of their pure forms respectively [93].

Seza, A. et al. presented microwave assisted synthesis of g-C_3N_4/SnO_2 by simple pyrolysis of urea. It is the first ever synthesis of g-C_3N_4 using microwave assistance, wherein urea is converted to g-C_3N_4 nanorod, and then the uniform distribution of SnO_2 over the surface makes it a promising material for visible light photoactivity to be used for water splitting [94]. Jingran Xiao, et al., prepared g-C_3N_4 on ZnO wires, and then incorporated nano clusters of Pt over the surface. Both the g-C_3N_4 and ZnO act as photo anodes while Pt carries the charges generated; i.e., electrons generated. This showed great improvement in the photoactivity in sun light; the efficiency increased by 9.5 times that of ZnO pure and 4.5 times that of g-C_3N_4/ZnO. The recombination of electron holes further reduced by the newly formed anode with Pt over surface. Composites of ZnO and g-C_3N_4 were prepared and nano-clusteres were decorated over the surface, which eventually increased the performance [95]. Feng Guoa et al., formed another heterojunction of g-C_3N_4 with CoO; studies showed that this metal oxide decoration over the surface of graphite carbon nitrite increased the photo activities of the newly formed photocatalyst.

The formation of this hetero-conjunction catalyst was done through the "solvothermal" process. Among all of the combinations, 30 wt% CoO and g-C_3N_4 had H_2 evolution rates of 50.2 μmol/g·h and 27.8 μmol/g·h for O_2 evolution [96]. Kelin He et al. fabricated a nano-heterojunction co-catalyst system based on the doping of hexagonal Ni_3C nanoparticles produced by thermolysis at low temperature on the base g-C_3N_4 nanosheets via simple grinding method. The catalyst comprising of over 15 wt% Ni_3C content showed the hydrogen production rate of 1518 μmol/g·h when irradiated with visible light and an apparent quantum yield 116 fold greater than pure g-C_3N_4; i.e., 0.4% at 420 nm successfully showing better results than noble metal 0.5 wt% Pt/g-C_3N_4 sample. This relatively low cost, good performance, non-noble metal addition of co-catalyst enables a decrease in hydrogen production over-potential, improvement in oxidation kinetics and effective charge carrier separation [97]. Another Non-noble metal alternative with superior hydrogen evolution rate of 169 μmol/g·h has been reported by Lu Chen et al. The technique centered on the combination of Ni_3N nanoparticles and g-C_3N_4 nanosheets via a hydrothermal method and subsequent annealing step which ensures stabilization of Ni_3N structures on g-C_3N_4 and maintains the hydrogen productivity. The notable advantages of this material include the lower cost, higher throughput than 3 wt% Pt/g-C_3N_4 material, multiple cycles operation, better carrier separation and visible light operation. These properties are attributed to the optimal loading and distribution of Ni_3N active co-catalyst medium and better stability of Ni_3N phase with a minimal conversion to less active Ni or $Ni(OH)_2$ states [98]. Based on the single layer fabrication and promising scalable strategy of single layer SnS_2 nanosheets of 3-atom thickness exhibiting above 38% water splitting efficacy under visible light by Yongfu Sun et al. Shao-hua Chen et al. further investigated the prospects of coupling SnS_2 nanosheets with g-C_3N_4 to overcome the performance limitations of afore-mentioned research. The results were conformed with the intended improvements of better charge carrier separation and band alignment owing to the weak Vander Walls heterojunction between SnS_2 and g-C_3N_4 [99]. Another approach using environmentally benign materials and methods was introduced by Rongchen Shen et al., in which the hybridization of Co_2P nanoparticles formed from phosphorization technique of cobalt metal organic framework and g-C_3N_4 nanosheets. The resulting g-C_3N_4/Co_2P/K_2HPO_4 material formed by simple grinding method exhibited a 556 times superior H_2 production rate compared to simple g-C_3N_4, i.e., 556 μmol/g·h, owing to the lower hydrogen production over potentials, better light absorbance, diminished charge carrier combination tendency and provision of an alternate reaction pathway by proton-reduction [100]. A recent approach to produce cobalt phosphide (CoP)/g-C_3N_4 cocatalysts has been presented by Xiao-Jun Sun et al., involving dual-step calcination of ZIF-67. The calcination was carried out to formulate CoP nanoparticles, which were found to boost the hydrogen release rate to as high as 201.5 μmol/g·h with a meager NPs loading of 1.42 wt%. ZIF-67 was formulated by the traditional method and g-C_3N_4 by melamine thermal condensation; they were subsequently combined, ground and calcined at a high temperature. The H_2 release rate exhibited a directly proportional relation with increasing ZIF-67 concentration until 5 wt% (1.42% CoP), indicating deterrence in ability to absorb light. Moreover, the lower water contact angle of the hybrid material than those of the individual components conforms to the assumption of better water absorption ability and reduction of adsorbed proton specie. These factors, along with the notably lower charge transport resistance indicated by photocurrent experiments, contribute to the exemplary alliance and compatibility of CoP and g-C_3N_4 as photocatalysts [101]. Another methodology to incorporate graphite carbon nitride as a root material was verified by garnishing carbon based quantum dots on g-C_3N_4 nano-tubes by thermal co-polymerization method. Yang Wang et al. reported the resultant hydrogen release rate as high as 3538.3 μmol/g·h due to reduced charge recombination and greater light capturing capabilities, demonstrating 10.94% quantum yield. The co-condensation of these components encourages tube arrangement and micro-sized composite structure to stimulate transfer of photoelectrons. Introduction of C-QDs notably shifted the pure g-C_3N_4 nano-sheet structure towards nano-tube structure, because of the tough amide bonds created among C-QDs and urea precursor. Furthermore, the band gap of untreated base material was shifted from 2.70 to 2.60 eV due to the structural change and multi-reflective containment of incident light radiations in the nano-tubes [102].

Nan Wang et al., in their research, developed MnO_2 with a co-modified nanocarbon tube with a g-C_3N_4 ternary composite. Different properties were studied, and the compound was characterized by different conventional techniques. It was observed that this ternary compound shows more active photocatalysis in contrast with carbon nanotubes (CNTs)/C_3N_4. Here, CNTs capture the electrons generated when light falls over the surface of this catalyst, which resultantly increases the rate of water splitting; hence, more hydrogen is formed. Hydrogen production is increased with rate of 4067 µmol/g·h [103]. Figure 5 shows the composite g-C_3N_4/GO with MoS2 as potential photogenerated carrier separator.

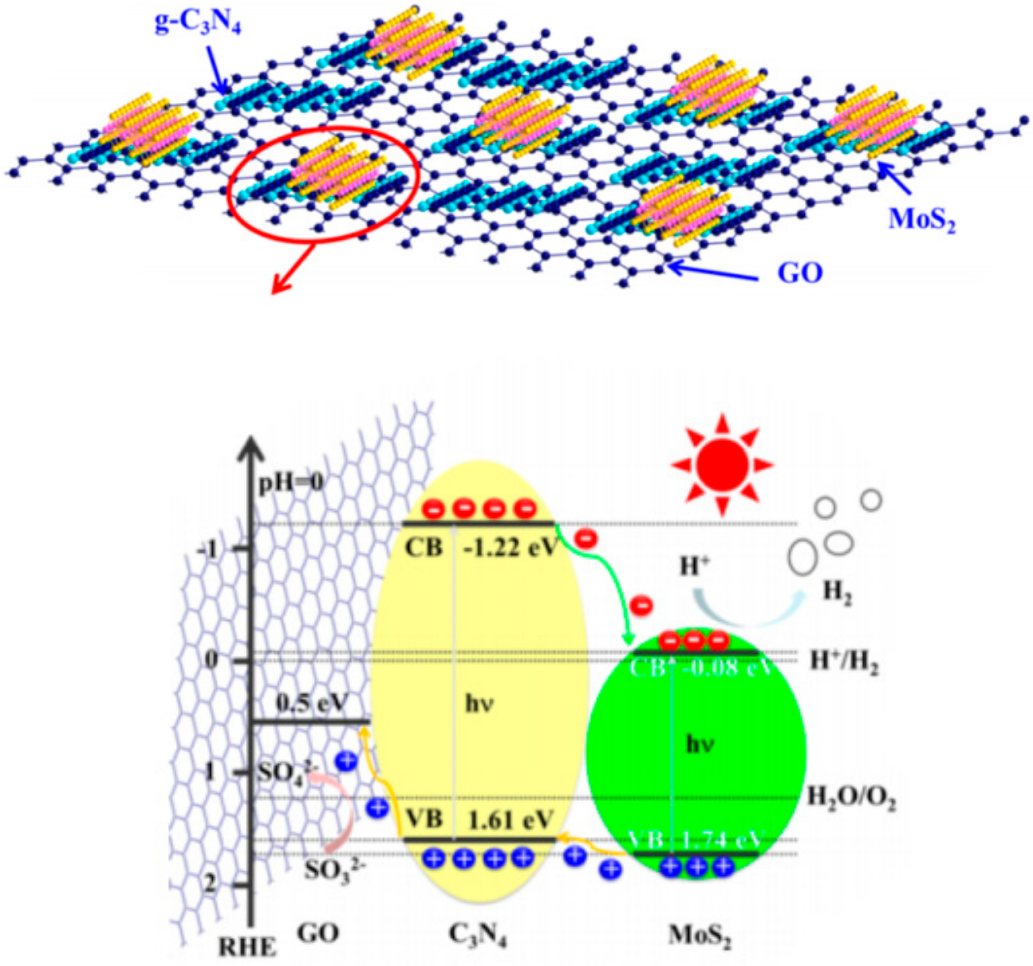

Figure 5. Schematics of MoS2/g-C_3N_4/GO composite and charge carrier separation. (Reprinted with permission from [104]. Copyright (2017), American Chemical Society).

2.2. *Graphene-Based Photocatalysts for Water Splitting*

Another metal-free photocatalyst for photocatalytic water splitting activity is graphene. It has gotten immense attention recently. In 2004, demonstration of the "sticky-tape peeling" of atomically thin sheets of carbon atoms from a mass of graphite brought a revolution in 2D materials research. This thinnest-ever material is known as "graphene" [105]. It is characterized by excellent chemical, mechanical and electrical properties [106]. For example, graphene is 100 times harder than steel; superior to copper in terms of electrical and thermal conductivity; and is flexible and transparent. Proposed future applications include uses ranging from computer chips and flexible displays to batteries and fuel cells [107].

Graphene is proving to be a potential candidate for the production of hydrogen, due its low cost and environmentally friendly nature, and shows unique charge carrier mobility properties, large specific

surface area (single layer: 2650 m^2/g) [108], high transparency, structural flexibility, chemical stability and unique optoelectronic properties [109]. Graphene has been established as a viable and efficient material choice for improved catalytic operation with various other semi-conducting materials [29] due to its extended two-dimensional sp^2 hybrid carbon network framework structure. It offers excellent electron transporting and accepting characteristics, due to which it behaves as a multi-dimensional passageway for electrons, and hence, helps to effectively separate the photo-generated charge carriers. However, the possibility and efficacy of graphene to transport electron holes is yet to be explored and studied. Moreover, a great number of established studies have been concentrated on combinations of a single type of nanoparticle and graphene film, for use as photocatalysts to improve hydrogen gas production (Figure 5); but the incorporation of two or more components as co-catalysts on graphene for greater selectivity and improved performance has not been achieved. Graphene can be produced via top down or bottom up approach (Figure 6) and synthesis methodology effects the intrinsic property of the graphene. The atomically thin and flexible graphene layers can not only provide a support for dispersing metallic or oxide nanoparticles and provide a highly conductive matrix, but also can induce easier electron transfer from the conduction band of semiconductors to graphene due to large energy level offset formed at the interface, leading to an efficient charge separation.

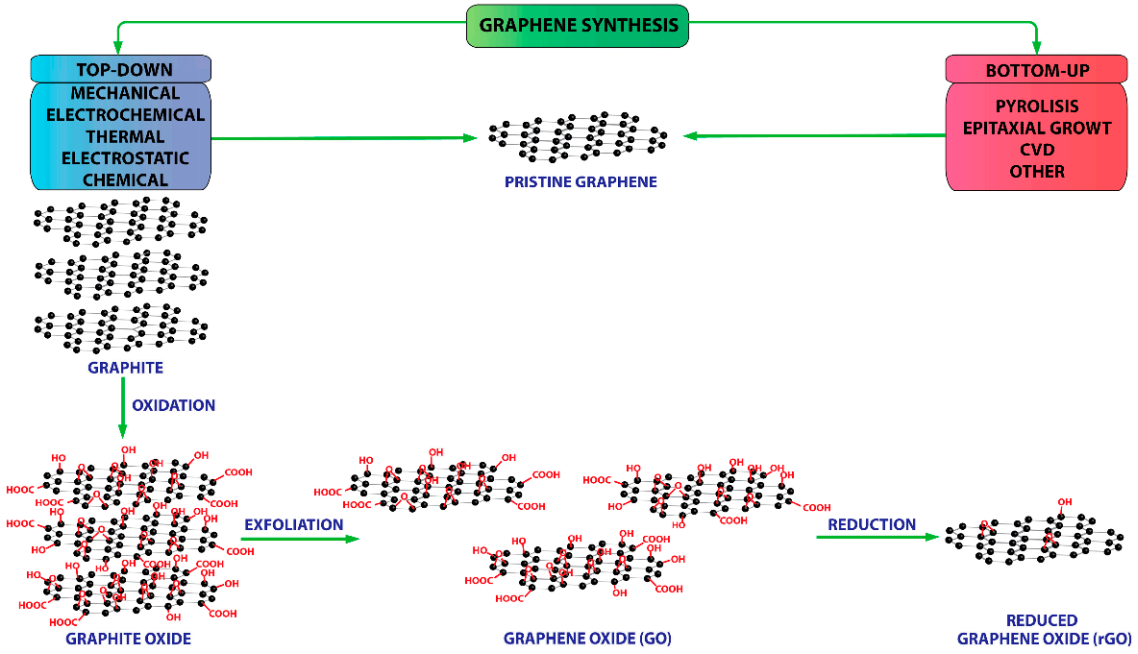

Figure 6. Top-down and bottom-up synthesis schematics of graphene. (Reprinted from [110], Copyright (2017), MDPI).

The different structures of graphene have been explored to enhance the photocatalytic performance of graphene. Graphene can be only used with a combination of other materials due to its lack of a natural band gap. Yibo Yan et al. prepared functionalized graphene quantum dots to improve performance [111]. Since the development of photocatalytic technology, TiO_2 has been a photocatalyst due to its high efficiency, low cost and good stability. TiO_2/graphene composites are currently being considered as one of the promising candidates for photocatalytic applications. The study by Angel Pérez del Pino et al. is focused on developing an inexpensive, metal-free, eco-friendly and benign photo-active catalyst while eliminating unsafe metals and reagents with superior efficiency and practicability. Laser-exposure leads to the development of defects in lattice structure, crinkles and holes, nitrogen integration, reduction of GO recognized by a drop-in oxygen atoms attached to GO and a rise in carbon content. It was further ascertained that the proliferation in N-content in GO structure results in better charge segregation, hydrogen liberation and photo-catalytic efficacy. Thus, it was logically

concluded that the favorable factors for improving performance are nitrogen content assimilated in graphene and a degree of reduction, because redox reactions are favorably promoted by carbon adjacent to pyridinic-N. A hydrogen gas production rate of up to 89.29 µmol/L was recorded [112]. Shixiong Min et al. prepared TiO_2–rGO–CoO_x advanced photo-catalyst via two step hydrolysis-thermal process to separately integrate TiO_2 and CoO_x species on rGO sheets. Despite the direct non-participation of rGO as a catalyst in redox processes in water splitting, its incorporation results in noteworthy increases in gas production rates and catalytic activity due to its quality of greater electron and hole kinetics, translating to lower charge combination and transportation of electrons from TiO_2, and hole transport to CoO_x [113]. Cheng, P., and Yang, Z. et al., improved the performance of typical photocatalyst TiO_2 by combining it with graphene, which has unique properties, such as flexible structure, huge specific surface area, high transparency and electron mobility, making it a worthy contender to be combined with TiO_2 to improve its photoactivity. The experimental results specified the solvothermal reduction of graphene oxide to graphene sheets, thereby augmenting the light absorption ability of P25–GR nanocomposites and also their charge separation efficiency. Graphene played the role of photogenerated electron acceptor due to its 2D π-conjugation structure and helped as an effective transporter in the separation of electron–hole pairs. The hybrid displayed superior activity towards the evolution of hydrogen from methanol solution under the illumination caused by Xe-lamp when compared to bare P25 due to improved ability for light absorption and a lower electron–hole pair recombination rate (Figure 7). The examination of photocatalytic activity of P25–GR nanocomposites based on graphene content affirmed a mass ration of 0.5 wt% GR to P25 as the optimum, with further addition of graphene leading to a decreased photocatalytic activity [39]. Li et al. worked to enhance photo-activity of traditional TiO_2-rGO promoter and introduce an innovative method to fabricate these materials which is environmentally friendly, single-step, intense chemical-free and upgrades the gas production capability of the system by dropping band gap energy. The absence of surface Ti^{3+} species and its presence in the bulk of the sample results in better performance with respect to H_2 liberation, creation of an alternate e-conduit, modifying the reaction from UV to the visible spectrum and absorbing charge transporters. Materialization of titanium–carbon bonds leads to reducing the band gap of titanium oxide, expanding the photosensitivity range, declining the charge conduction resistance and facilitating conduction between rGO and TiO_2 (Figure 8). Hydrogen productivity grew with increasing rGO content and laser exposure duration. Peak H_2 formation rate recorded was 16000 µmol/g·h and solar transformation efficiency was 14.3%, which were the subsequent outcomes of strongly coupled TiO_2 and rGO components [91].

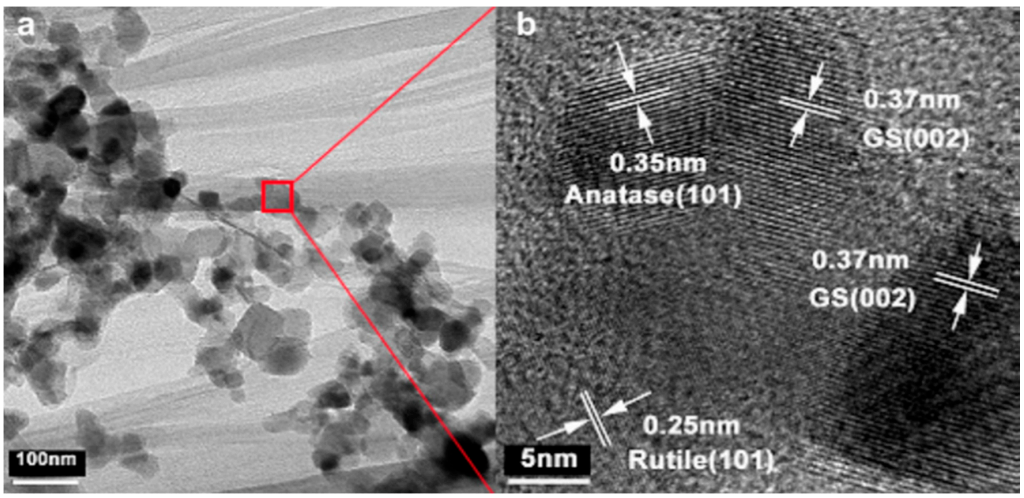

Figure 7. TEM image (**a**) and HRTEM image (**b**) of P25–10%GR [39]. (Reprinted from Int. J. Hydrogen Energy, Volume 37, Cheng P., et al., TiO_2–graphene nanocomposites for photocatalytic hydrogen production from splitting water, Pages 2224–2230. Copyright (2012), with permission from Elsevier).

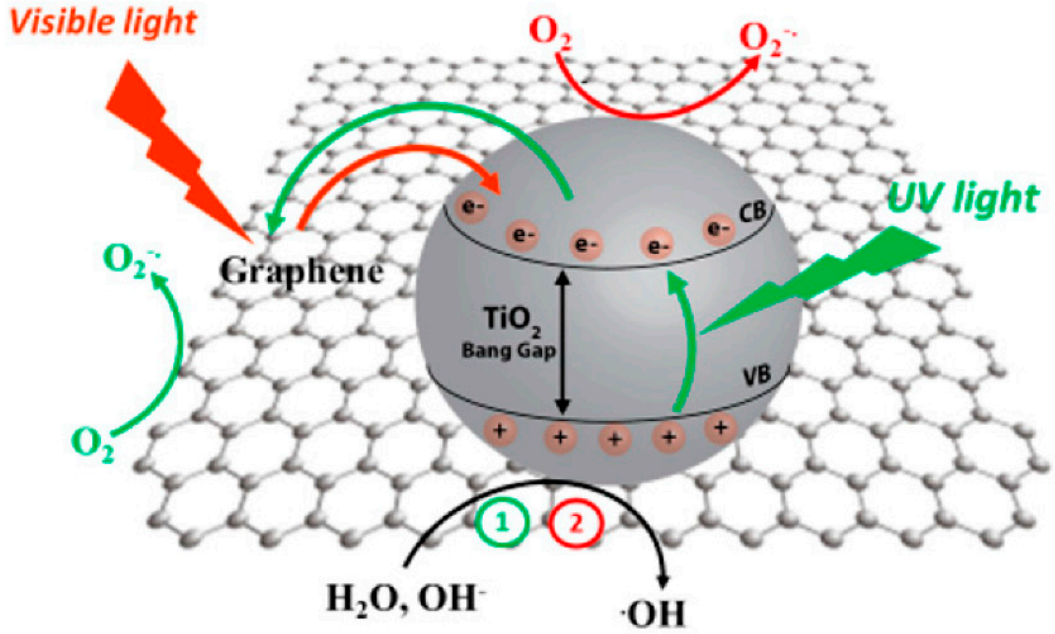

Figure 8. Mechanisms of UV and visible light activation of TiO_2 with graphene. (Reprinted from [110], Copyright (2017), MDPI).

Sankeerthana Bellamkonda et al. studied unique photocatalytic composites of graphene and carbon nanotube amalgamations of semiconductor materials. The linking of reduced TiO_2-x facets with carbon matrix exhibited the extraordinary photoactivity for the dissociation of water to produce hydrogen at room temperature. These nanohybrid composites produced hydrogen at 29,000 µmol/g·h, with 14.6% solar energy conversion efficiency, to hydrogen. The augmented photoactivity of this nanohybrid composite is ascribed to O_2 vacancies on the surface, the presence of Ti^{3+} sites in the TiO_2 lattice and the interfacial interaction between TiO_2 and graphene [114]. Multi-layers of graphene result in increased light absorption, and the formation of 111 oriented gold nanoplatelets on multilayer graphene was analyzed by Diego Mateo et al. The orientation of incorporated Au NPs was detected using XRD and EDX. The hydrogen and oxygen production rates noted were 12,000 and 9000 µmol/g·h respectively. When compared with previous literature using similar materials, it was concluded that the enhanced rates were a result of using specialized one-step synthesis process along with the highly oriented attachment of Au particles on graphene material, which affected the strength of interactions, ability of charge separation and the photo-catalytic performance [115]. Mohamed, Mokhtar et al. found that energy conversion efficiency is also prohibited in most of these metal oxides due to their high band gap energies (E_g). To mitigate such problems, spinel families, AFe_2O_4 (A = Co, Cu, Zn) have been examined as photocatalysts for H_2 production; particularly, manganese ferrite ($MnFe_2O_4$) hybridized with graphene/graphene oxide to decrease E_g and particles size, and to enhance both electronic conductivity and surface area. Enhanced light absorption ability of these hybrids induced more charge carriers, thereby increasing their apparent quantum efficiency to work as photocatalysts for water splitting. A nanospindle-shaped GO1:Mn1 hybrid absorbed more visible light for the stated purpose of generating high current density values exceeding traditional semiconductors, which improved its performance as a photocatalyst [116]. Katsuya Iwashina et al. studied the photo-catalytic activity for water splitting using the rGO-TiO_2 composite (oxygen-producing promoter) as an electron-transfer facilitator and sulfide-metal materials as hydrogen-producing promoters. Sulfide metal materials in unaided form are unfitting for direct use for water-splitting promoters due to issues relating to photo-corrosion. However, when combined with semiconducting materials for hydrogen production and using rGO-TiO_2 functionalized material for oxygen liberation, efficient gas production was observed. This scheme is also feasible for use in solar-aided reactions. Loading of noble metal co-catalysts with sulfide metals affected the activity owing to the particle sizes and

extents of distribution. Moreover, the incorporation of platinum via adsorption showed the highest photo-catalytic character [117]. Zhenhua Pan et al. made RGO overcome the charge transfer challenge between loaded catalyst specks on a conductive sheet by introducing reduced graphene oxide as an arbitrating redox binder. The degree of reduction is an established factor in determining the equilibrium between hydrophilicity and conductive ability necessary for a photo-active material, which was ascertained in this case by XPS and Raman spectroscopy. The water dissociation rate was enhanced 3.5 fold by the incorporation of rGO in catalytic sheets, when compared to those that were devoid of rGO under identical circumstances, due to its inherent property of assisting in charge transmission. The role of Au as mechanical support and protection against self-oxidation was reiterated by results. Moreover, rGO helped in robust fixation of other active particulates on the Au sub-layer. Increasing its content to 1.25% (optimum) led to gradual growth in effectiveness, but a further rise in GO content caused the undesired excessive coverage of active species. Furthermore, the samples with superior dispersion of particulates presented an extra boost in efficiencies by as much as 1.7 times [118]. Graphene oxide (GO) based hybrid materials could be employed in several applications, including hydrogen generation. Carbon-based 2D structures processed by graphene oxide and its reduced form have controllable, layered structures; huge surface areas; and tunable optical, electronic and magnetic properties. Certain orthodox photocatalytic materials, such as Pt, TiO_2, ZnS and CdS, could be dispersed onto these GO/rGO matrices, resulting in efficient hybrids for less energy intensive H_2 production via photocatalytic water dissociation reaction. Doping of metal ion, particularly Co^{2+} and Al^{3+}, considerably enhanced the production of hydrogen by rGO, indicating that efficient photocatalyst could be synthesized using simple hybrids of rGO and transition metal ions [119]. A novel combination of materials was studied by Xiujun Fan, et al. Nano-crystals of three transition metal carbides were enclosed in thin graphene nano-ribbons via hot filament chemical vapor deposition technique to obtain highly pure Fe, Co and Ni carbides supported on the peaks of graphite thorn-like upright nano-ribbon structure. The stimulating hierarchical structure produced inspired a comprehensive and relative study of the sizes, shapes and other dispersion factors of carbides on 2D graphene vertical conical arrays. The GNRs not only act as a supporting substrate to enhance stability but also prevent the aggregation of carbides on the surface, holding them well into place. The porous channels also expedite the electron transport to the core, causing a distinct decline in conduction resistance. The suitability of these materials for ORR has been indicated by ample reduction of oxygen at low Tafel slopes of 39, 41 and 45 mV/dec for Fe, Co and Ni carbide GNRs, respectively—comparable to 32 mV/dec value for Pt/C electrode. The HER current densities produced by M_3C-GNRs (M = Fe, Co, Ni) were 166.6, 79.6 and 116.4 mA/cm^2 at 200 mV over-potential. These operative statistics can be ascribed to the coupled carbide-graphene effects of high roughness factors, large active area exposure and superior conducting ability and porosity of graphene [120].

2.3. Phosphorene

Phosphorene is a two dimensional (2D) material with a band gap of 0.3 to 2 eV from bulk phosphorus (Figure 9) to single layer phosphorene. The band gap of phosphorene is tunable depending on applied strain. The properties of phosphorene change with change in stress, number of layers and applied electric field [121,122]. It consists of singled-layer black phosphorus, is similar to graphene, is included in the family of monolayer-flatland materials and arranged in a hexagonal puckered lattice [50,123].

Figure 9. The layered and anisotropic crystal structure of elemental black phosphorus. (Reprinted with permission from [41]. Copyright (2015), Elsevier).

The advantage of phosphorene over graphene is that it shows a band gap. Black phosphorous was discovered around 100 years ago, but the discovery of phosphorene is just over four years old. Therefore, very little experimental research of phosphorene has been reported [124]. A monolayer of black phosphorous (BP) was synthesized using the sticky-tape technique used earlier for graphene; the material was titled phosphorene. Phosphorene has the promising properties of niche 2D materials. It shows the quantum confinement effect in a direction perpendicular to the 2D plane, which induces distinct electronic and optical properties; natural passivation of the surface without any dangling bond; no lattice mismatch concerns for assembling vertical heterostructures with other 2D materials; a high specific surface area; and a strong interaction with light. These properties are considered extremely necessary for photocatalytic applications. Additionally, phosphorene has a tunable band gap and shows anisotropic properties that make it suitable for a variety of applications [125]. Black phosphorous is the most stable allotrope of phosphorous. It has layered in-plane strong bonds along with weak van der Waals interlayer interactions. This layered structure provides the opportunity for fabrication of very thin layers of phosphorous by exfoliation from a bulk size. The techniques which have been reported for the fabrication of phosphorene so far are based on micromechanical cleavage using sticky-tape and solvent exfoliation methods. Single layer phosphorene has also been fabricated by combining mechanical exfoliation with plasma thinning technique. This sticky-tape micro mechanical exfoliation can yield phosphorene of high crystal quality, but with very low product density. In order to avoid chemical degradation, black phosphorus must be exfoliated using anhydrous and oxygen-free solvents such as acetone, chloroform, isopropyl alcohol or dimethyl form-amide. The technique of exfoliation with sonication results in low cost and a high yield of 2D phosphorene. It also seems feasible as a process for development in large scale production. However, it becomes practical only if there is a good matching of the surface tension between the layer crystal and the solvent, and if the solvent can stabilize the nanosheet to evade restacking and aggregation. Phosphorene shows a highly anisotropic structure in nature. The monolayer structure of black phosphorus is a 2D material; however, its excitonic properties closely resemble quasi-1D material, such as carbon nano-tubes. Similar to bulk black phosphorus, phosphorene shows quantum confinement perpendicular to the 2D plane. The band gap of phosphorene can be modulated appropriately for photon absorption in the ultraviolet to the near-infrared region of the solar spectrum. Apart from theoretical studies, there is actually very little published work that proves the water splitting capability of phosphorene, conclusively, at the laboratory scale [126]. However, some work has been done for phosphorene hybrids with various oxides, graphene and few sulfides. The hybrid of black phosphorous and TiO_2 has been reported as a photocatalyst in the quest for improved activity as shown in Figure 10. It was demonstrated that when bare BP was irradiated by visible light, it increased its degradation after various runs. However, when TiO_2 was loaded to form TiO_2/BP hybrid, the degradation was reduced by 90%. The reason for the improved stability can be described as due to the substitution of Ti atoms into the BP matrix to make BP

resistant to moisture or oxygen. This study suggests that alteration of phosphorene with semiconductor materials might be a solution to increase the stability of phosphorene to ambient degradation and phosphorene can better be used as a photocatalyst [127]. In addition to BP/TiO_2, BP/SnO_2, BP/WO_3 and other oxides also need to be investigated, as no research has been published yet. Yongqing Cai et al. reported that graphene could be suitable as a supporting layer for encapsulating phosphorene to improve interaction and provide collaborative effects. This hybrid combination needs in depth study to find conclusive findings [128]. The eminent ability of black phosphorus nano-sheets to employ the solar energy efficiently (approximately 75%) in photocatalytic operation and the superior charge separation capacity of cobalt phosphide (CoP) can effectively be integrated in a single material, as supposed by Bin Tian, et al. [129]. The synthesis procedure consists of a straightforward solvo-thermal step involving white phosphorus and a Co-source (Co $(NO_3)_2{\cdot}6H_2O$) instead of the relatively tedious, expensive and complicated procedure of bulk BP synthesis and later exfoliation to nano-sheets. The special effects of CoP addition on BP resulted in manifold increase in H_2 release rate, 30 before and 735 µmol/g·h after CoP addition. MoS_2/phosphorene and WS_2/phosphorene hybrids demonstrate type II heterostructures. Type II is more expedient for electron-hole separation than type I and type III. The band gap of MoS_2/phosphorene varies between 0.59 to 1.06 eV, whereas it varies between 0.90 to 1.44 eV for the WS_2/phosphorene hybrid [130]. It seems that MoS_2/phosphorene cannot be used as a water splitting photocatalyst because its band gap is much below the thermodynamics band gap requisite of 1.23 eV for a photocatalyst [131]. Very little work has been done for phosphorene/sulfide hybrids. Other potential 2D sulfides/phosphorene hybrids, such as CdS/phosphorene, CdSe/phosphorene and WS_2/phosphorene, are yet to be explored. However, sulfide compounds are easily degradable in water, as they get irradiated by light. Hence, along with band gap congruency, stability is also major drawback with sulfides photocatalyst materials [132].

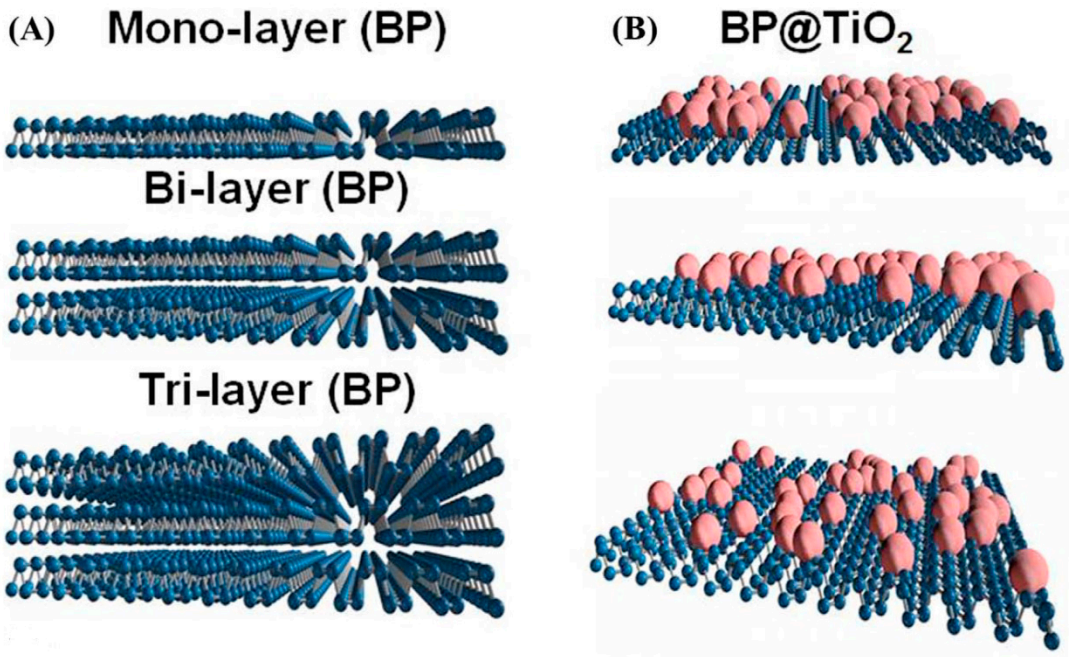

Figure 10. TiO_2 substitution on BP [127]. (Reprinted with permission from Lee, H.U., et al., Sci. Rep., 2015. 5: p. 8691).

2.4. Metal Phosphides

Phosphides of many transition metals are emerging as very popular photocatalysts due to their ability to adsorb hydrogen atoms and release H_2 gas, easily proving themselves to be very practical HER (hydrogen evolution reaction) catalysts, as confirmed by Shi and Zhang [133]. Furthermore, their tuneability to perform as dual function catalysts has been investigated via co-catalysis mechanism

to enhance both HER and OER processes by incorporation of metal hydroxo/oxo groups on material surfaces. Nickel, cobalt and iron phosphides and their binary and ternary derivatives have been tried and tested by many researchers for photocatalytic applications and have showed promising outcomes. The P-content in the metal catalyst material has been suggested as a major deciding factor in determining the HER activity of material, as it is found to be responsible for the catalyst's interaction and affinity with H atoms. This trend has been reported by Yuan Pan et al. [134] and Sengeni Anantharaj, et al. [135], who confirmed the direct relation between HER catalytic activity and P content; i.e., an increase in the P ratio results in a corresponding increase in activity as well as in release rate. The OER's (oxygen evolution reaction) activity depends principally on the optimal bond energy values of the interaction between catalytic material and reaction intermediates (oxide, peroxide and hydro peroxide). Nickel phosphide was investigated as a dual functional photocatalyst by Marc Ledendecker, et al. [136]. It showed high activities for both HER and OER, attaining 10 mA/cm^2 under 1.7 V. Ni_5P_4 nanostructure was grown directly on Ni-sheets by an extremely straightforward process involving the heating of elemental phosphorus and Ni-foil sheet under inert conditions. The material showed good performance for the especially imperative OER kinetics, which is normally a challenging task in photocatalysis. This feature can be the consequence of formation of highly active NiOOH intermediate deposition on the surface which contributes to reduce the operation over-potential, the shift in electronic structure, superior current density and stable operation in a 20-h test conditions in acidic environment [136]. An alternate variation of nickel phosphide, Ni_2P as a potential electrode catalyst was suggested by Lucas A. Stern, et al. [137], wherein the active specie was found to promote both the HER and OER kinetics presenting an economically feasible and efficient single-material substitute catalyst. The Ni_2P nanoparticles and nanowires were fabricated through simple and scalable heating of the precursor ingredients, both of which showed comparable OER activities. The detailed structural studies showed the shell/core structure of NiO_x/Ni_2P which contributes prominently in the process as the Ni_2P core offers an electronic passageway to the NiO_x shell, thereby providing better diffusive characteristics and improved activity as compared to equivalent sized NiO_x nanoparticles. The reported values of current density 10 mA/cm^2 achieved with overpotential were as insignificant as 290 mV for OER and 10 mA/cm^2, with 136 mV overpotential for HER in acidic medium driving the developed catalyst material towards the mainstream photocatalytic water splitting systems as a promising and practical candidate material for both anodic and cathodic reactions [137]. Apart from nickel, other transition metal phosphides have also been investigated for catalysis to release hydrogen and oxygen from water by using incident light source. Cobalt phosphides emerged as a stimulating opportunity in this regard, and several reviewers and researchers have explored the utility of different forms and combinations of Co phosphides. Yang Y, et al. [138] formulated cobalt centric thin sheets via an intricate multistep process involving plasma cleaning of glass plate substrate, sputter-coating conduction nano-layers of chromium (10 nm) and gold (40 nm), Co-layer deposition by aqueous plating solution of $CoSO_4$, formation of porous thin Co-oxide layer by anodic treatment of Co-layer under static voltage and then finally chemical vapor deposition of phosphorus for conversion to Co-phosphide while conserving the regular porous film (500 nm thickness). The ratio of film active area to the electrode surface area (denoted by roughness factor) was calculated as a parameter to endorse the high activity of material without the necessity of external additives. Hence, the proposition was confirmed by an observed increase in RF from six (compact-before anodic treatment) to 95 (highly porous). The operational tests showed steady operation and an exceptional HER activity of 30 mA/cm^2 at overpotentials of 175 mV (in acidic condition) and 430 mV (under basic conditions) which is even higher than most noble metal based contemporary catalysts, such as CoP nanoparticles (20 mA/cm^2), Co/CNT (10 mA/cm^2), MoP (10 mA/cm^2), Ni_2P (20 mA/cm^2) and C_3N_4 (10 mA/cm^2). Similarly, notable results were observed in terms of OER activity as well; i.e., current density of 30 mA/cm^2 at 330 mV overpotential which is again higher than most up-to-date studied catalysts, such as CoP nanoparticles (25 mA/cm^2), Au/Co_3O_4 (25 mA/cm^2) and most ternary selections as well [138]. A valuable comparative analysis of different raw materials for CoP fabrication and their effectiveness in

terms of HER efficiencies as scrutinized by Afriyanti Sumboja, et al. [139] to provide an outlook for large-scale and commercially applicable source of CoPs manufacture. Salts such as cobalt acetate and cobalt acetylacetonate were phosphodized by sodium hypophosphite in a single-step. The CoP formed from the former ingredient exhibited better HER promotion (overpotentials: 160 mV in acidic, 175 mV in basic media) due to greater phosphide fraction (92.5%) and greater surface area (ECSA: 10–15 cm^2). While the latter being a readily oxidizable salt produces a greater fraction of metallic Co rather than phosphide (63.5% CoP), lower surface area (ECSA: 7–12.5 cm^2) and greater overpotential (169 mV in acidic, 188 mV in basic media) [139]. The application of Co-phosphide nanosheets as HER promoter in 1M KOH media has been studied by Liang Su, et al. [140] wherein the novel approach of effects of surface refurbishment of CoP nanosheets are exposed. The CoP nanosheets were conventionally synthesized by phosphidation of Cobalt oxides and then engineered electrochemically to promote an irrevocable and stable transformation into $Co(OH)_x$/CoP hybrid configuration that displayed excellent HER catalysis producing 10 mA/cm^2 with 100 mV overpotential as compared to the untreated CoP nanosheet overpotential of 180 mV. The dispersion of hydroxyl group on the nanosheet surface as an outcome of 10 hours' exposure to 20 mA/cm^2 exhibit a coarser surface, greater turnover frequency of 0.234 per second and reliable operation even after 5000 cycles. These improvements in performance by the surface modification are attributed to the arrangement of $Co(OH)_x$ complexes which are efficient promoters of the breakdown of water into molecular components. As this stage is the rate-determining step of HER mechanism, this surface makeover of CoP nano-sheets proves to be highly favorable for the process and the copiously released H-atoms interact with adjoining CoP molecules to release hydrogen gas readily. The merger of both $Co(OH)_x$ and CoP specie is most beneficial for the process as compared to single-component systems as established by the comparative assessment of $Co(OH)_x$/CoP (100 mV overpotential), untreated CoP (180 mV) and C_3N_4 (300 mV) samples [140]. CoP nano-rods supported on Nickel foam as reported by Yun-Pie Zhu, et al. [141] is a novel strategy to fabricate dual-function HER and OER promoters with high efficacy, high porosity, enhanced diffusive transport and surface area (148 m^2/g) while maintaining high conductivity. The synthesis procedure revolves around potentio-deposition of nanorods on Ni-foam while the CoP deposited is produced in situ, facilitated by direct electron passageways provided by Ni-foam. Current densities of 10,100 and 800 mA/cm^2 at 54, 121 and 235 mV overpotentials for HER and 100 mA/cm^2 for overall cell voltage of 1.62 V were accomplished which are even more efficient than Pt and IrO_2 system [141]. Ternary variants, such as Ni-Co-P have also been developed successfully to integrate the desired properties of component materials. Yingjie Li, et al. [142] cultivated Ni-Co-P nano-sheet arrangements on Ni foam by two stage hydrothermal and phosphorization scheme. The synthesized material demonstrated extraordinary performance for both HER and OER catalysis even when compared with the traditional commercially used noble metal (Pt/C, Ir/C) electrodes and the separately tested Ni_2P and Co_2P nano-sheet arrays produced by the same method. The overpotential values for Ni-Co-P ternary electrodes for HER and OER were 133 and 308 mV respectively necessary to operate at 50 mA/cm^2 and the cell voltage required was as minimal as 1.77 V. The remarkable activity and stability of material can be credited to marginal electron resistance, normalized hydrogen binding forces, material's inherent high activity and a distinctive super-aerophobic nano-framework [142].

A similar arrangement was prepared by Liang H, et al. [143] with plasma-facilitated growth of Ni-Co-P on Ni foam, concluding in a menial over-potential of 32 mV for HER and 280 mV for OER with 10 mA/cm^2 current density and 1.58 V cell potential. Bi-functional high porosity Ni-Co-P nano-sheet catalyst supported on carbon-fiber paper was developed by Rui Wu, et al. [144] by electrodeposition resulting in identical sheet arrangements with subsequent annealing to generate spongy $Ni_{0.1}Co_{0.9}P$ structure. The annealing temperature, Ni: Co ratio of 1:9 and the precursors were deciding factors for optimal synthesis of active material. The detailed characterization results indicated that resulting material operated at high turn-over frequency (0.24 per sec for H_2, 0.12 per sec for O_2), reliable stability (20 h operation, 1000 cycles), better electron transmission ability and interactive sites contributed by Ni fraction and high efficiency. Cell voltage required for operation at 10 mA/cm^2 was a competitive

value of 1.89 V and the over-potential was 125mV as compared to 174 and 196 mV for CoP and Ni_2P electrodes [144]. An ample amount of laudable work in the ternary Ni-Co-P catalyst and its composites category can be mentioned such as NiCoP/Carbon cloth composite as dual function catalyst reported by Cheng Du, et al. [145], with overpotentials as petite as 44 and 62 mV for HER and OER respectively at 10 mA/cm^2 current density and 1.77V cell potential for 100 mA/cm^2 output paves the way for practical non-noble metal electrode materials. NiCoP/r-GO composite for stimulating both HER and OER synthesized by Jiayuan Li, et al. [146] presented 10 mA/cm^2 current density with cell voltage 1.59V with stable operation for more than 75 hrs. The coupling of Co-doping in Ni_2P and their combination with rGO resulted in a boost in electron transport, catalytic activity and surface arrangement of active spots. An elegant and novel heterostructure involving NiCoP@Cu_3P nano-sheets was cultivated on Cu foam by Xingxing Ma, et al. [147] as a favorable candidate for both HER and OER catalysis showcasing 54 mV and 309 mV over-potentials for HER and OER at 10 mA/cm^2. Similarly an intricate system of NiCoP nano-sheets grown on N-doped Carbon-coated Ni foam as formulated by Miaomiao Tong, et al. [148] through hydrothermal and phosphorization route required 31.8 mV and 308.2 mV for HER and OER to accomplish 10 mA/cm^2 current density. The durable performance and activity experiments showed comparable outcomes to the commercial Pt/C and Ru_2O catalysts.

2.5. Metal Organic Frameworks and Derivatives

Metal organic framework or MOF is the peculiar category of crystalline synthetic materials that has claimed a prominent position in the league of modern multi-functional materials due to the distinctive properties of high porosity, adaptable pore structures, larger surface area and amendable elemental compositions. MOFs comprise of a network assembly of metal centers linked to organic bridging ligands which result in a variety of geometries, compositions and pore spacing dependent upon the synthesis procedure, conditions and initiators. The unique metal-centric interlinked geometric morphology allows MOF applications in various fields including, but not limited to, gas adsorption and separation, catalysis, drug delivery systems, optics and sensors [149–157] and the possibilities and opportunities of its efficient utilization and improvements are continuously being analyzed by researchers every day [158,159]. Numerous MOF-based catalyst materials have been synthesized, characterized and upgraded for photocatalytic water splitting reactions in recent times [160,161] with a focus to develop novel and feasible bi-functional promoters to make the concept of commercial solar hydrogen production from water a practical reality [162]. The standard practices to convert MOFs into practical photocatalysts comprise of inclusion of light-sensitive building blocks into the MOF backbone for instance aminoterephthalates [163,164] and porphyrins [165], Doping with any active metal or noble metal in order to enhance catalytic capacities [166], inorganic nano-particles encapsulated in MOFs [167], assembling ternary composites and introduction of electron donor or trapping materials to prevent charge recombination challenges [168]. A primary perspective of efforts in this regard will be presented herewith. The long-standing fact of high activity of noble metals in water splitting systems photocatalytically was incorporated into MOF-based materials by Meng Lan, et al. [169] to generate 3 types of Pt-tempered heterojunctions; i.e., Pt-ZnS-CoS, Pt-Zn_3P_2-CoP and Pt-ZnO-Co_3O_4. The synthesis procedure involved the ternary steps of Zn-Co ZIF preparation by previously reported methods [170–173], the sulfidation, phosphorization or oxidation of base ZnCo ZIF for each sample separately and the subsequent doping of Pt nano-particles. The twin-metal ZIF backbone facilitates the light absorption ability, increases the active area contact and favors charge carrier transportation and separation, while the dispersed Pt particles capture the electrons and motivate the hydrogen production. The resulting hydrogen release rates by above listed hetero-junctions are 8210, 9150 and 7800 μmol/g·h respectively. In the structural analysis, it was noted that the polyhedral MOF shape and porosity was retained after Pt-doping as well and the operational durability was noted to be unaffected even after 5 cycles. Cheng Wang, et al. [174] reported the fabrication of two kinds of Zr-carboxylate MOFs by intricate methods and their subsequent center-doping with Pt-nanoparticles whereby the produced Pt@MOF material displayed the ability to catalyze HER, recyclable nature by

simple centrifugation and the turnover number of 7000. Another example of incorporating Pt into MOF units for enhanced activity has been reported by Dengke Wang, et al. [175] wherein, the Pt nano-particles were disseminated uniformly via a novel photo-reduction method in MIL-100(Fe) MOF which has formerly been established as a water stable and photo-excitable material [176]. The introduction of optimal fraction of Pt (0.8%) in MOF structure verified the hydrogen release increase from 5.9 to 109 µmol/g·h (18.5 times of pristine MOF). This prime value is observed due to the collaborating mechanism of electrons generation by photo-active MOF structure and the immediate electron seizing by central Pt also acting as the prime H_2 production site. This coordinated functioning results in enhanced charge separation without compromising on the exposed excitation area of for light. Qin Liu, et al. [177] used a permeable Ni-foam as a substrate to utilize its conductive capacity, high exposed surface region and ease of electronic diffusion through the channels towards the active dispersed Ni-MOF arrays which allowed the current capacity to reach 100 mA/cm^2 at 320 mV over-potential and turnover frequency of 0.25 mol/s O_2. The in-situ hydrothermally grown Ni-MOF nano-sheet arrays on Ni-foam was analyzed thoroughly and compared to commercial Ru_2O/NF OER catalyst and simple NF (Nickel foam). The results displayed the trends of lower Tafel slope 123 mV/dec than NF (193 mV/dec) but higher than Ru_2O/NF (72 mV/dec) due to the different OER mechanisms followed by these materials. Faradaic efficiency measured for oxygen release by contrasting the theoretical and practically released oxygen was nearly 100% with a stable operation for 20 h test time endorsing its practicality as a successful OER promoter. In 2016, ultra-thin nano-sheets of bi-metallic NiCo MOF were prepared with a purpose to promote oxygen discharge from water by Shenlong Zhao, et al. [178]. Utilization of nano-sized ultra-thin MOF sheets introduces the merits of lower mass transport resistance, better electronic pathways for conduction, superior exposure to the remote active sites and un-bound highly active free metal sites which act in combination with the intrinsic effectiveness of Ni and Co base metals in OER catalysis. The 2D NiCO, ultra-thin MOF nano-sheets supported on Co-sponge exhibited reassuring performance with over-potential 189 mV at 10 mA/cm^2, continuous and stable operating time of 200 h and Faradaic efficiency of 99.3%. These parameters verified the hypothesized collective benefits of incorporating two-metals in MOF network and the working decision to use ultra-thin MOF structure on a porous support. A similar study using a different combination of metals, i.e., Ni-Fe ultrathin (≈3.5 nm) MOF nano-sheets, was conducted by jingjing duan, et al. [179]. This Ni-Fe combo also showed superior analytical parameters due to the identical structural and elemental choices as previously listed work. The over-potential observed in this case was 240 mV for 10 mA/cm^2 with noteworthy turnover frequency of 3.8 per sec and stable efficient operation for 20000 s. A three-component engineered MOF structure was developed by Rui Lin, et al. [180] that combined established photo-active ingredients to make a strong partnership of UiO-66 MOF, CdS and reduced graphene oxide. Inspired to resolve the electron-hole recombination challenge in CdS photocatalysts, combining CdS/rGO composite with UiO-66 MOF not only resolved this issue but added the benefits of its high contact area, considerable thermal stability [181] uniform pore channels and proven photo-active nature of UiO-66 for hydrogen production [182]. Consequently, the UiO-66/CdS/1%-rGO combination showed the best charge separation capacity as compared to other proportions of rGO and the hydrogen release 13.8 times superior to pristine CdS. Another variation of ternary MOF photocatalyst is based on MoS_2/UiO-66/CdS fusion structure [183] which delivered 32,500 µmol/g·h H_2 release rate. A CdS/MOF combination was developed to promote H_2 evolution reaction by Jiao He, et al. [184] with the unusual idea of supporting CdS active material on photocatalytically inert MIL-101 MOF defining its sole purpose of providing greater exposed active area. MIL-101 has Cr centric structure with benefits of excellent air, water and heat stability. The supported CdS@MOF formed a crystalline cubic shape and the highest H_2 release rate was noted for 10 wt% proportion on CdS reaching upto 75,500µmol/g.h. Another specimen using MIL-101 was prepared by amine sensitization along with Pt co-catalyst doping in 2014 to obtain greater hydrogen efficiency and stability [185]. Furthermore, Co-oxide restrained in MIL-101 was prepared by intricate method involving double solvo-thermal technique to create a robust material (TOF: 0.012/sec per Co-atom) with a rich oxygen

productivity (88%) [186]. The inventive strategy to produce a photo-sensitive MOF combination was explored to directly synthesize the MOF using dye-resembling organic azobenzene tetra carboxylic acid as an organic ligand and the metal (Gd) salt as the central backbone element. Xiaojun Sun, et al. [187] used a solvo-thermal method to synthesize yellow colored Gd-MOF crystals which were later also metal-laden with Ag (1–2%) as a second catalyst. The experimental comparison showed 154.2 μmol/g·h H_2 release from pristine Gd-MOF and 212 μmol/g·h from Ag (1.5%)/Gd-MOF under UV–Vis exposure due to the introduction of electron-trapping noble metal nature. Ag proved to be a suitable and feasible option as a noble metal dopant due to its cost effectiveness, lower electron transport resistance and decreased charge re-combination by capturing excited electron species released from photoactive MOF [188]. An alternate approach to integrate the qualities of superior photo-sensitivity, high HER activity and larger exposed surface area is to prepare syndicate of materials serving these purposes as formulated by Jiao He, et al. [189] wherein, a light sensitive Cr MOF UiO-66 was loaded with Pt nano-particles for HER activity and rhodamine B (RhB) dye for photo-activation. The impact of this fusion is clearly evident from H_2 evolution rates whereby pure UiO-66 displayed no perceptible H_2 release, Pt/UiO-66 showed 3.9 μmol/g·h and adsorbed RhB/Pt/UiO-66 showed 116 μmol/g·h which is 30 times greater than un-treated Pt/UiO-66. A different photo-active MOF variant MIL-125-NH_2 for H_2 production from water can be used as the base material with a MoS integration, as discovered by Tu N. Nguyen, et al. [190], to produce H_2 evolution rate as high as 2094 and 1454 μmol/g·h with quantum productivity 11% and 5.8% using two different kinds of MoS clusters; i.e., Mo_3S_{13} and IT-MoS respectively. MoS_2 is an inherently photo-active compound [191] and the sources of light responsive behavior are the vacancy defects and sulfur-edges only [192,193] while the basal faces do not contribute in catalysis and the size of particles is inversely related to the HER activity [194] Robust interaction between the supporting MOF and MoS result in higher exposed active area, lower electron conduction resistance and high stability. In an innovative approach to replicate the active nodular-structure of [NiFe] hydrogenase complex [195], a two-dimensional layered photo-responsive MOF $[Ni_2(PymS)_4]_n$ was fabricated via cautiously supervised multi-step hydrothermal process [196]. The resultant material showed robust water and air stability, bi-atomic Ni webbed morphology with 4 $PymS^-$ linkers and turnover frequency of 10.6 per hour and hydrogen release upto 6017 μmol/g·h using TEA as electron source, flourescien as photo-activator and white LED or visible light as source. The pH of solution, nature of sensitizer, nature of electron source and amount and particle size of catalyst were observed to be the deciding factors to determine the practical competence of the catalyst. A dual function catalyst with the aim of promoting both HER and OER components of the water dissociation process has many advantages and has been a center of research since decades now. A MOF-based route to achieve this goal was proposed by Yang An, et al. [169]. Pt and CoPi components were dispersed onto the innately photo-active MIL-125 (Ti) MOF [131] to boost hydrogen and oxygen discharge and suppress charge recombination tendency by the deposited components. The experimental H_2 and O_2 liberation rates under UV–Vis exposure were 42.33 and 21.33 μL/h. Separate influence of trace materials on the half-reactions were confirmed by appraising the MIL-125 (Ti) with CoPi@MIL-125 (Ti) and Pt@MIL-125 (Ti), which verified that the OER activity of CoPi-activated sample amplified to 307 μL/h from 143 μL/h, whereas in case of HER, introduction of Pt on MOF increased the activity 25 fold. Furthermore, the order of Pt and CoPi doping is a significant factor as a higher activity was noted when Pt was loaded first. Recently, an aluminum-centric MOF devised from 2-aminoterephthalic acid (ATA) was recognized as an active oxygen evolution promoter and modification of this material with Ni assimilation resulted in a dual purpose (HER and OER) overall water dissociation catalyst [197]. The half reaction analysis validated the coordinating nature of both Al and Ni components as OER for Al-ATA-Ni MOF was 5166.7 μmol/g·h contrasted with 550 μmol/g·h and HER for Al-ATA-Ni MOF was 1200 μmol/g·h and the material without Ni was found inactive towards hydrogen production. A bipyridine-centered MOF-253 was modified by confining Pt complex into the network with the intention to promote HER and simultaneously act as a photo-exciter [198]. The base MOF-253 possesses the anticipated merits of high exposed area and promising stability [199], which is evident in the

resulting compound and the addition of Pt component translates to five times increase in photo-activity. Another Ti-centric MOF was amended by incorporating Ru-complex established on the similar strategy to promote HER in visible light presence [200]. Despite being a relatively new concept and material, 2D MOFs have found various application in electrocatalysis, photocatalysis and heterogeneous catalysis in general [201]. The focus on optimization of manufacturing procedure, product stability, surface coating and immobilization techniques and scalability can bring this novel category of materials into limelight for future catalytic processes due to the inherent benefits of exposed active sites, turnover frequencies, effective coordinated properties of metal and organic ligands and easy handling capability.

3. Conclusions and Future Outlook

A tremendous amount of research and development has been carried out to improve, study and implement various strategies in photocatalytic water splitting using different categories of materials, composites, heterojunctions and immobilizing schemes, as summarized in Table 2 [202,203]; however, the use of 2D materials, their combinations and derivatives is a developing concept in photocatalytic water splitting research, which poses itself as an excellent opportunity for advancement and further exploration of innovative materials. With tunable and unique architectures, distinctive features and desirable structural intricacies being the specialties of 2D materials, it seems imperative to delve into this arena for progressive photocatalysis systems. Keeping these positive outlooks and prospects in view, this review highlights the evolution of modern nanomaterials, 2D photocatalysts and MOF derivatives to attain the coveted properties of low charge recombination, high photo absorbance activity, efficient electron conductivity, fast kinetics and large surface area for water splitting to produce hydrogen. It has been concluded that production of hydrogen can be enhanced using various techniques, including doping with noble metal particles, surface functionalization, nano-heterostructures, synthesis-controlled morphology and surface decoration of nano-particles in 2D cages. The most common backbone materials noted in this regard are the graphitic carbon nitride, and graphene, which serve as supporting pillars and high area foundations in case of composite materials and hetero-structural modifications. Meanwhile, phosphorene has emerged as a relatively novel material and limited research has been done to explore the possibilities of practical application of this material. Metal phosphides and metal organic frameworks have been extensively incorporated in 2D heterostructures and as supporting cocatalysts to improve performance and functional enhancement of base materials and assure performance improvement with further research and experimentation. With the acknowledgement of the fundamentally essential properties displayed by the 2D base materials and their variants, as discussed in this article, it is safe to conclude that photocatalytic research and the commercial application of this promising technology has found 2D materials and their hybrids to be promising and stimulating candidates. However, despite the progress in research, the challenges associated with 2D materials present an opportunity to explore improvements in existing 2D materials and the development of new alternatives with novel electronic and structural features, such as electrochemically reduced thin films (e.g., α-Fe_2O_3) [28], layered oxyhalides (FeOBr, Bi_4VO_8Cl, etc.), thiophosphates ($CoPS_3$), metal chalcogenides, 2D MOFs and metal-free semiconducting materials [46]. Moreover, the setbacks associated with cost effective, bulk production of these ultrathin photocatalysts limits the scalability for prospective commercial operation which needs to be addressed and resolved. The odds of bulk scale synthesis from nano-layered and non-layered materials to manufacture 2D thin sheets must be improved to make thickness-controlled and efficient 2D photocatalysts. Debottlenecking of issues related to stability in water splitting reaction conditions, such as agglomeration, corrosion and oxidation, must be prioritized to explore surface deformation control and reduction of surface energies. Fast charge carrier re-combination could be mitigated by sacrificial agents, but better practicality demands investigation of alternative solutions, such as 2D/2D, 2D/1D and 2D/0D heterojunctions to introduce interfacial charge separation. Modern systems and industries thrive on the basis of technology; thus, optimization and simulation tools must be introduced to foster research and development in photocatalysis and eliminate the gap between theoretical and real-time reaction systems.

Table 2. Summary of photocatalytic water splitting systems discussed in this article involving g-C_3N_4, graphene, phosphine, metal phosphides and metal organic frameworks MOFs.

Photocatalyst	Bandgap (eV)	Thickness (nm)	Co-Catalyst	Sacrificial Agent	Light Source	Type of Reaction	Activity (μmol/g·h)	Ref.
g-C_3N_4 nanosheet	2.85	-	3 wt% Pt	15 vol% TEOA, $AgNO_3$ (0.1 M)	300 W Xenon lamp, λ > 420 nm cutoff filter	HER OER	297 120	[85]
Br modified g-C_3N_4	2.82	-	3 wt% Pt, 0.3 wt% CoOx	10 vol% TEOA, $AgNO_3$ (0.01 M)	300 W Xenon lamp, λ > 420 nm cutoff filter	HER OER	600 80	[86]
Ti_3C_2/g-C_3N_4 Heterojunction	2.77 of g-C_3N_4 nanosheets	1.7–2.6	3 wt% Pt	10 vol% TEOA	200 W Hg lamp, λ > 400 nm cutoff filter	HER	72.3	[89]
$NiTiO_3$/g-C_3N_4	2.18 $NiTiO_3$, 2.7 g-C_3N_4	-	1 wt% Pt	10 vol% TEOA	300 W Xenon lamp, λ > 420 nm cutoff filter	HER	835	[90]
O-doped g-C_3N_4 nanosheets	2.95	-	3 wt% Pt	-	300 W Xenon lamp, λ > 400 nm cutoff filter	HER	3786	[91]
WO3 decorated g-C_3N_4	2.39	-	-	10 vol% glycerol	500 W Xenon lamp	HER	1111	[92]
$KNbO_3$/g-C_3N_4 Heterojunctioon	-	-	2 wt% Pt	5 vol% TEOA	300 W Xenon lamp	HER	1019.38	[93]
CoO/g-C_3N_4 Heterojunctioon	2.52 CoO, 2.75 g-C_3N_4	-	-	-	White LED, λ > 400 nm	HER OER	50.2 27.8	[96]
Ni_3C/g-C_3N_4 Heterojunctioon	2.65	-	15 wt% Ni_3C	15 vol% TEOA	350 W Xenon lamp, λ > 420 nm cutoff filter	HER	1518	[97]
Ni_3N/g-C_3N_4 Heterojunctioon	-	-	3 wt% Ni_3N	10 vol% TEOA	300 W Xenon lamp, λ > 400 nm cutoff filter	HER	169	[98]
Co_2P/g-C_3N_4	2.61	-	2 wt% Co_2P	15 vol% TEOA, 0.1mM K_2HPO_4 proton carrier	300 W Xenon lamp	HER	556	[100]
ZIF-67 derived CoP/g-C_3N_4	2.85	-	1.42 wt% CoP	-	Light irradiation λ > 320 nm	HER	201.5	[101]
MnO_2/CNT/g-C_3N_4	2.64	-	MnO_2/CNT	-	70 W metal halide lamp (380 nm < λ < 780 nm)	HER	4067	[103]
GO thin film/MoS_2/g-C_3N_4 Quantum dots	1.82 MoS_2, 2.83 g-C_3N_4	-	MoS_2/g-C_3N_4 Quantum dots	0.25 M Na_2SO_3	450 W Xenon lamp	HER	1650	[104]
TiO_2/CoOx/rGO nanosheet	-	-	TiO_2 nanoparticles/CoOx	20 vol% CH_3OH, 0.05 M $AgNO_3$	250 W Hg lamp	HER OER	3800 1616	[113]
TiO_2/Graphene nanosheet	2.96	1	0.5 wt% Pt	25 vol% CH_3OH	300 W Xenon lamp	HER	6680	[39]
CNT/Graphene/TiO_2 nanohybrid	2.79	7	Graphene	10 vol% CH_3OH	350 W Xenon lamp	HER	29,000	[114]

Table 2. *Cont.*

Photocatalyst	Bandgap (eV)	Thickness (nm)	Co-Catalyst	Sacrificial Agent	Light Source	Type of Reaction	Activity (μmol/g·h)	Ref.
111-oriented Au nanoplatelets/Graphene	-	20	Au nanoplatelets	TEOA	150 W Xenon lamp	HER OER	12,000 9000	[115]
rGO-transition metal hybrids	-	-	Al, Co, Fe, Ni, Mn	-	500 W Xenon lamp	HER	24.74	[119]
Black Phosphorus/Monolayer Bi2WO6 Nanosheets	0.3–2 eV BP, 2.67 MBWO	-	3 wt% Pt	-	Visible light	HER	4208	[125]
BP/CoP nanosheets	1.14	1.4	CoP	None	300 W Xenon lamp, λ > 420 nm cutoff filter	HER	735	[129]
Pt@UiO-66-NH_2 MOF	2.76	-	2.87 wt% Pt	TEOA, CH_3CN	Visible light	HER	257.38	[155]
Pt/Amine functionalized Ti-MOF	-	-	Pt	0.01 M TEOA	Xenon lamp, λ > 420 nm	HER	366.7	[164]
Co_3O_4/TiO_2 heterojunction using Co-MOF sacrificial template	-	-	2 wt% Co	15 vol% CH_3OH	400 W Xenon lamp	HER	7000	[168]
Pt heterojunction using bimetallic MOF template	-	-	Pt	10 vol% CH_3OH	300 W Xenon lamp	HER	9150	[169]
Pt/MIL—100(Fe)	-	-	0.8 wt% Pt	CH_3OH (1:3,CH_3OH:H_2O)	300 W Xenon lamp, λ > 420 nm cutoff filter	HER	109	[175]
UiO-66/CdS/1%rGO	-	-	Pt	0.1 M Na_2S, 0.1 M Na_2SO_3	300 W Xenon lamp, λ > 400 nm cutoff filter	HER	13,800	[180]
MoS_2/UiO-66/CdS hybrid	-	-	1.5 wt% MoS_2	10 vol% LA	300 W Xenon lamp, λ > 420 nm cutoff filter	HER	32,500	[183]
CdS(10wt%)/MIL-101	-	-	0.5 wt% Pt	LA	Visible light λ > 420 nm	HER	75,500	[184]
Pt/NH_2-MIL-101(Cr)	-	-	1.5 wt% Pt	25 vol% TEOA	Visible light	HER	50,000	[185]
MoS/MIL125-NH_2	1.29 MoS_2	-	0.8 wt% $Mo_3S_{13}^{2-}$, 1T-MoS_2	16.1 vol% TEA	Xenon lamp λ > 420 nm	HER	2094, 1454	[190]
2D Ni mercaptopyrimidine MOF	-	-	-	15 vol% TEA	White LED	HER	6017	[196]
Al-based MOF derived from 2-aminoterephthalic acid	2.75	-	Ni^{2+}	CH_3OH, $AgNO_3$	Xenon lamp	HER OER	1166.7 5000	[197]

Author Contributions: All authors have contributed to the research work. Z.S. and M.U.Y. are masters students and both have written this paper under the supervision of E.P. She gave the main idea to the students about writing a comprehensive review article related to very emerging field of water splitting and guided students about how to write. M.B.K.N. have helped us a lot in grammatical purview and proof reading. All authors have read and agreed to the published version of the manuscript.

Funding: This research is funded by Higher Education Commission (HEC) Pakistan, financial grant no 2017/HEC/NRPU/10482 and APC was funded by National University of Sciences & Technology (NUST), Islamabad Pakistan.

Acknowledgments: Author Erum Pervaiz would like to acknowledge NUST Pakistan and the HEC project (2017/NRPU-10482) for financial support.

Conflicts of Interest: All authors have mutually agreed upon this submission and there is no conflict of interest that needs to be declared.

References

1. Lewis, N.S.; Nocera, D.G. Powering the planet: Chemical challenges in solar energy utilization. *Proc. Natl. Acad. Sci. USA* **2006**, *103*, 15729–15735. [CrossRef] [PubMed]
2. Zou, C.; Zhao, Q.; Zhang, G.; Xiong, B. Energy revolution: From a fossil energy era to a new energy era. *Nat. Gas Ind. B* **2016**, *3*, 1–11. [CrossRef]
3. Resch, G.; Held, A.; Faber, T.; Panzer, C.; Toro, F.; Haas, R. Potentials and prospects for renewable energies at global scale. *Energy Policy* **2008**, *36*, 4048–4056. [CrossRef]
4. Uyar, T.S.; Beşikci, D. Integration of hydrogen energy systems into renewable energy systems for better design of 100% renewable energy communities. *Int. J. Hydrogen Energy* **2017**, *42*, 2453–2456. [CrossRef]
5. Tachibana, Y.; Vayssieres, L.; Durrant, J.R. Artificial photosynthesis for solar water-splitting. *Nat. Photonics* **2012**, *6*, 511. [CrossRef]
6. Momirlan, M.; Veziroglu, T. Current status of hydrogen energy. *Renew. Sustain. Energy Rev.* **2002**, *6*, 141–179. [CrossRef]
7. Ismail, A.A.; Bahnemann, D.W. Photochemical splitting of water for hydrogen production by photocatalysis: A review. *Sol. Energy Mater. Sol. Cells* **2014**, *128*, 85–101. [CrossRef]
8. Yao, L.; Wei, D.; Ni, Y.; Yan, D.; Hu, C. Surface localization of cdzns quantum dots onto 2D g-C_3N_4 ultrathin microribbons: Highly efficient visible light-induced H_2-generation. *Nano Energy* **2016**, *26*, 248–256. [CrossRef]
9. Zhou, C.; Zhao, Y.; Shang, L.; Shi, R.; Wu, L.-Z.; Tung, C.-H.; Zhang, T. Facile synthesis of ultrathin snnb2o6 nanosheets towards improved visible-light photocatalytic h2-production activity. *Chem. Commun.* **2016**, *52*, 8239–8242. [CrossRef]
10. Inoue, Y. Photocatalytic water splitting by ruo2-loaded metal oxides and nitrides with d0- and d10 -related electronic configurations. *Energy Environ. Sci.* **2009**, *2*, 364. [CrossRef]
11. Zheng, Y.; Jiao, Y.; Jaroniec, M.; Qiao, S.Z. Advancing the electrochemistry of the hydrogen-evolution reaction through combining experiment and theory. *Angew. Chem.* **2015**, *54*, 52–65. [CrossRef] [PubMed]
12. Liang, B.; Zhang, N.; Chen, C.; Liu, X.; Ma, R.; Tong, S.; Mei, Z.; Roy, V.A.L.; Wang, H.; Tang, Y. Hierarchical yolk–shell layered potassium niobate for tuned ph-dependent photocatalytic h2 evolution. *Catal. Sci. Technol.* **2017**, *7*, 1000–1005. [CrossRef]
13. Wang, Y.; Wang, X.; Antonietti, M. Polymeric graphitic carbon nitride as a heterogeneous organocatalyst: From photochemistry to multipurpose catalysis to sustainable chemistry. *Angew. Chem.* **2012**, *51*, 68–89. [CrossRef] [PubMed]
14. Osterloh, F.E. Inorganic nanostructures for photoelectrochemical and photocatalytic water splitting. *Chem. Soc. Rev.* **2013**, *42*, 2294–2320. [CrossRef]
15. Pan, Z.; Hisatomi, T.; Wang, Q.; Chen, S.; Nakabayashi, M.; Shibata, N.; Pan, C.; Takata, T.; Katayama, M.; Minegishi, T.; et al. Photocatalyst sheets composed of particulate lamg1/3ta2/3o2n and mo-doped bivo4 for z-scheme water splitting under visible light. *ACS Catal.* **2016**, *6*, 7188–7196. [CrossRef]
16. Zhao, Y.; Zhang, J.; Li, K.; Ao, Z.; Wang, C.; Liu, H.; Sun, K.; Wang, G. Electrospun cobalt embedded porous nitrogen doped carbon nanofibers as an efficient catalyst for water splitting. *J. Mater. Chem. A* **2016**, *4*, 12818–12824. [CrossRef]
17. Hisatomi, T.; Domen, K. Reaction systems for solar hydrogen production via water splitting with particulate semiconductor photocatalysts. *Nat. Catal.* **2019**, *2*, 387–399. [CrossRef]

18. Ida, S.; Ishihara, T. Recent progress in two-dimensional oxide photocatalysts for water splitting. *J. Phys. Chem. Lett.* **2014**, *5*, 2533–2542. [CrossRef]
19. Coronado, J.M. A Historical Introduction to Photocatalysis. Design of Advanced Photocatalytic Materials for Energy and Environmental Applications. In *Green Energy and Technology*; Springer: London, UK, 2013; pp. 1–4.
20. Lee, Y.Y.; Jung, H.S.; Kang, Y.T. A review: Effect of nanostructures on photocatalytic co 2 conversion over metal oxides and compound semiconductors. *J. CO2 Util.* **2017**, *20*, 163–177. [CrossRef]
21. Wang, Q.; Hisatomi, T.; Suzuki, Y.; Pan, Z.; Seo, J.; Katayama, M.; Minegishi, T.; Nishiyama, H.; Takata, T.; Seki, K.; et al. Particulate photocatalyst sheets based on carbon conductor layer for efficient z-scheme pure-water splitting at ambient pressure. *J. Am. Chem. Soc.* **2017**, *139*, 1675–1683. [CrossRef]
22. Hisatomi, T.; Kubota, J.; Domen, K. Recent advances in semiconductors for photocatalytic and photoelectrochemical water splitting. *Chem. Soc. Rev.* **2014**, *43*, 7520–7535. [CrossRef] [PubMed]
23. Su, T.; Shao, Q.; Qin, Z.; Guo, Z.; Wu, Z. Role of interfaces in two-dimensional photocatalyst for water splitting. *ACS Catal.* **2018**, *8*, 2253–2276. [CrossRef]
24. Li, Y.; Li, Y.-L.; Sa, B.; Ahuja, R. Review of two-dimensional materials for photocatalytic water splitting from a theoretical perspective. *Catal. Sci. Technol.* **2017**, *7*, 545–559. [CrossRef]
25. Acar, C.; Dincer, I.; Naterer, G.F. Review of photocatalytic water-splitting methods for sustainable hydrogen production. *Int. J. Energy Res.* **2016**, *40*, 1449–1473. [CrossRef]
26. Tewari, V.K.; Zhang, Y. (Eds.) nanostructured two-dimensional materials. In *Modeling, Characterization, and Production of Nanomaterials*; Woodhead Publishing: Cambridge, UK, 2015; pp. 477–524.
27. Peng, R.; Ma, Y.; Huang, B.; Dai, Y. Two-dimensional janus ptsse for photocatalytic water splitting under the visible or infrared light. *J. Mater. Chem. A* **2019**, *7*, 603–610. [CrossRef]
28. Wang, J.; Waters, J.L.; Kung, P.; Kim, S.M.; Kelly, J.T.; McNamara, L.E.; Hammer, N.I.; Pemberton, B.C.; Schmehl, R.H.; Gupta, A.; et al. A facile electrochemical reduction method for improving photocatalytic performance of α-fe2o3 photoanode for solar water splitting. *ACS Appl. Mater. Interfaces* **2017**, *9*, 381–390. [CrossRef]
29. Jafari, T.; Moharreri, E.; Amin, A.S.; Miao, R.; Song, W.; Suib, S.L. Photocatalytic water splitting-the untamed dream: A review of recent advances. *Molecules* **2016**, *21*, 900. [CrossRef]
30. Murashkina, A.A.; Bakiev, T.V.; Artemev, Y.M.; Rudakova, A.V.; Emeline, A.V.; Bahnemann, D.W. Photoelectrochemical behavior of the ternary heterostructured systems cds/wo3/tio2. *Catalysts* **2019**, *9*, 999. [CrossRef]
31. Navarro Yerga, R.M.; Alvarez Galvan, M.C.; del Valle, F.; Villoria de la Mano, J.A.; Fierro, J.L. Water splitting on semiconductor catalysts under visible-light irradiation. *ChemSusChem* **2009**, *2*, 471–485. [CrossRef]
32. Shen, S.; Shi, J.; Guo, P.; Guo, L. Visible-light-driven photocatalytic water splitting on nanostructured semiconducting materials. *Int. J. Nanotechnol.* **2011**, *8*, 523–591. [CrossRef]
33. Ahmad, H.; Kamarudin, S.; Minggu, L.; Kassim, M. Hydrogen from photo-catalytic water splitting process: A review. *Renew. Sustain. Energy Rev.* **2015**, *43*, 599–610. [CrossRef]
34. Agbe, H.; Nyankson, E.; Raza, N.; Dodoo-Arhin, D.; Chauhan, A.; Osei, G.; Kumar, V.; Kim, K.-H. Recent advances in photoinduced catalysis for water splitting and environmental applications. *J. Ind. Eng. Chem.* **2019**, *72*, 31–49. [CrossRef]
35. Yousaf, M.U.; Pervaiz, E.; Minallah, S.; Afzal, M.J.; Honghong, L.; Yang, M. Tin oxide quantum dots decorated graphitic carbon nitride for enhanced removal of organic components from water: Green process. *Results Phys.* **2019**, *2019*, 102455. [CrossRef]
36. Xing, J.; Fang, W.Q.; Zhao, H.J.; Yang, H.G. Inorganic photocatalysts for overall water splitting. *Chem. Asian J.* **2012**, *7*, 642–657. [CrossRef] [PubMed]
37. Kitano, M.; Hara, M. Heterogeneous photocatalytic cleavage of water. *J. Mater. Chem.* **2010**, *20*, 627–641. [CrossRef]
38. Kouser, S.; Thannikoth, A.; Gupta, U.; Waghmare, U.V.; Rao, C.N.R. 2D-gas as a photocatalyst for water splitting to produce h2. *Small* **2015**, *11*, 4723–4730. [CrossRef]
39. Niu, P.; Zhang, L.; Liu, G.; Cheng, H.-M. Graphene-like carbon nitride nanosheets for improved photocatalytic activities. *Adv. Funct. Mater.* **2012**, *22*, 4763–4770. [CrossRef]
40. Sun, Y.; Gao, S.; Lei, F.; Xie, Y. Atomically-thin two-dimensional sheets for understanding active sites in catalysis. *Chem. Soc. Rev.* **2015**, *44*, 623–636. [CrossRef]

41. Zhuiykov, S. Nanostructured two-dimensional materials. In *Modeling, Characterization and Production of Nanomaterials: Electronics, Photonics and Energy Applications*; Woodhead Publishing: Cambridge, UK, 2015; pp. 477–524.
42. Luo, B.; Liu, G.; Wang, L. Recent advances in 2d materials for photocatalysis. *Nanoscale* **2016**, *8*, 6904–6920. [CrossRef]
43. Lu, L.; Xu, S.; Luo, Z.; Wang, S.; Li, G.; Feng, C. Synthesis of znco2o4 microspheres with zn0.33co0.67co3 precursor and their electrochemical performance. *J. Nanopart. Res.* **2016**, *18*, 183. [CrossRef]
44. Low, J.; Cao, S.; Yu, J.; Wageh, S. Two-dimensional layered composite photocatalysts. *Chem. Commun.* **2014**, *50*, 10768–10777. [CrossRef] [PubMed]
45. Ye, S.; Wang, R.; Wu, M.-Z.; Yuan, Y.-P. A review on g-c3n4 for photocatalytic water splitting and co2 reduction. *Appl. Surf. Sci.* **2015**, *358*, 15–27. [CrossRef]
46. Di, J.; Xiong, J.; Li, H.; Liu, Z. Ultrathin 2d photocatalysts: Electronic-structure tailoring, hybridization, and applications. *Adv. Mater.* **2018**, *30*, 1704548. [CrossRef] [PubMed]
47. Su, T.; Qin, Z.; Ji, H.; Wu, Z. An overview of photocatalysis facilitated by 2d heterojunctions. *Nanotechnology* **2019**, *30*, 502002. [CrossRef]
48. Zhan, W.; Sun, L.; Han, X. Recent progress on engineering highly efficient porous semiconductor photocatalysts derived from metal–organic frameworks. *Nano-Micro Lett.* **2019**, *11*, 1. [CrossRef]
49. Liu, Y.; Liang, L.; Xiao, C.; Hua, X.; Li, Z.; Pan, B.; Xie, Y. Promoting photogenerated holes utilization in pore-rich wo3 ultrathin nanosheets for efficient oxygen-evolving photoanode. *Adv. Energy Mater.* **2016**, *6*, 1600437. [CrossRef]
50. Lei, F.; Sun, Y.; Liu, K.; Gao, S.; Liang, L.; Pan, B.; Xie, Y. Oxygen vacancies confined in ultrathin indium oxide porous sheets for promoted visible-light water splitting. *J. Am. Chem. Soc.* **2014**, *136*, 6826–6829. [CrossRef]
51. Sun, Y.; Sun, Z.; Gao, S.; Cheng, H.; Liu, Q.; Lei, F.; Wei, S.; Xie, Y. All-surface-atomic-metal chalcogenide sheets for high-efficiency visible-light photoelectrochemical water splitting. *Adv. Energy Mater.* **2014**, *4*, 1300611. [CrossRef]
52. Sun, Y.; Cheng, H.; Gao, S.; Sun, Z.; Liu, Q.; Liu, Q.; Lei, F.; Yao, T.; He, J.; Wei, S.; et al. Freestanding tin disulfide single-layers realizing efficient visible-light water splitting. *Angew. Chem.* **2012**, *51*, 8727–8731. [CrossRef]
53. Sun, Y.; Sun, Z.; Gao, S.; Cheng, H.; Liu, Q.; Piao, J.; Yao, T.; Wu, C.; Hu, S.; Wei, S.; et al. Fabrication of flexible and freestanding zinc chalcogenide single layers. *Nat. Commun.* **2012**, *3*, 1057. [CrossRef]
54. Xiong, J.; Wen, L.; Jiang, F.; Liu, Y.; Liang, S.; Wu, L. Ultrathin hnb3o8 nanosheet: An efficient photocatalyst for the hydrogen production. *J. Mater. Chem. A* **2015**, *3*, 20627–20632. [CrossRef]
55. Liu, Y.; Xiong, J.; Luo, S.; Liang, R.; Qin, N.; Liang, S.; Wu, L. Ultrathin hnbwo6 nanosheets: Facile synthesis and enhanced hydrogen evolution performance from photocatalytic water splitting. *Chem. Commun.* **2015**, *51*, 15125–15128. [CrossRef] [PubMed]
56. Huang, Z.; Zhao, Y.; Song, Y.; Li, Y.; Wu, G.; Tang, H.; Zhao, J. Study on the oxidation process of cobalt hydroxide to cobalt oxides at low temperatures. *RSC Adv.* **2016**, *6*, 80059–80064. [CrossRef]
57. Xu, Y.; Zhao, W.; Xu, R.; Shi, Y.; Zhang, B. Synthesis of ultrathin cds nanosheets as efficient visible-light-driven water splitting photocatalysts for hydrogen evolution. *Chem. Commun.* **2013**, *49*, 9803–9805. [CrossRef] [PubMed]
58. Yang, W.; Zhang, L.; Xie, J.; Zhang, X.; Liu, Q.; Yao, T.; Wei, S.; Zhang, Q.; Xie, Y. Enhanced photoexcited carrier separation in oxygen-doped znin2s4 nanosheets for hydrogen evolution. *Angew. Chem. Int. Ed.* **2016**, *55*, 6716–6720. [CrossRef] [PubMed]
59. Yang, S.; Gong, Y.; Zhang, J.; Zhan, L.; Ma, L.; Fang, Z.; Vajtai, R.; Wang, X.; Ajayan, P.M. Exfoliated graphitic carbon nitride nanosheets as efficient catalysts for hydrogen evolution under visible light. *Adv. Mater.* **2013**, *25*, 2452–2456. [CrossRef]
60. Li, J.; Zhan, G.; Yu, Y.; Zhang, L. Superior visible light hydrogen evolution of janus bilayer junctions via atomic-level charge flow steering. *Nat. Commun.* **2016**, *7*, 11480. [CrossRef]
61. Okamoto, Y.; Ida, S.; Hyodo, J.; Hagiwara, H.; Ishihara, T. Synthesis and photocatalytic activity of rhodium-doped calcium niobate nanosheets for hydrogen production from a water/methanol system without cocatalyst loading. *J. Am. Chem. Soc.* **2011**, *133*, 18034–18037. [CrossRef]
62. Huang, C.; Chen, C.; Zhang, M.; Lin, L.; Ye, X.; Lin, S.; Antonietti, M.; Wang, X. Carbon-doped bn nanosheets for metal-free photoredox catalysis. *Nat. Commun.* **2015**, *6*, 7698. [CrossRef]

63. Ida, S.; Kim, N.; Ertekin, E.; Takenaka, S.; Ishihara, T. Photocatalytic reaction centers in two-dimensional titanium oxide crystals. *J. Am. Chem. Soc.* **2015**, *137*, 239–244. [CrossRef]
64. Yang, M.Q.; Xu, Y.J.; Lu, W.; Zeng, K.; Zhu, H.; Xu, Q.H.; Ho, G.W. Self-surface charge exfoliation and electrostatically coordinated 2d hetero-layered hybrids. *Nat. Commun.* **2017**, *8*, 14224. [CrossRef] [PubMed]
65. Su, T.; Hood, Z.D.; Naguib, M.; Bai, L.; Luo, S.; Rouleau, C.M.; Ivanov, I.N.; Ji, H.; Qin, Z.; Wu, Z. 2d/2d heterojunction of ti3c2/g-c3n4 nanosheets for enhanced photocatalytic hydrogen evolution. *Nanoscale* **2019**, *11*, 8138–8149. [CrossRef] [PubMed]
66. Xu, Q.; Zhu, B.; Jiang, C.; Cheng, B.; Yu, J. Constructing 2d/2d fe2o3/g-c3n4 direct z-scheme photocatalysts with enhanced h2 generation performance. *Solar RRL* **2018**, *2*, 1800006. [CrossRef]
67. Tan, P.; Zhu, A.; Qiao, L.; Zeng, W.; Ma, Y.; Dong, H.; Xie, J.; Pan, J. Constructing a direct z-scheme photocatalytic system based on 2d/2d wo3/znin2s4 nanocomposite for efficient hydrogen evolution under visible light. *Inorg. Chem. Front.* **2019**, *6*, 929–939. [CrossRef]
68. Shi, J.; Li, S.; Wang, F.; Gao, L.; Li, Y.; Zhang, X.; Lu, J. In situ topotactic formation of 2d/2d direct z-scheme cu2s/zn0.67cd0.33s in-plane intergrowth nanosheet heterojunctions for enhanced photocatalytic hydrogen production. *Dalton Trans.* **2019**, *48*, 3327–3337. [CrossRef]
69. Fu, J.; Xu, Q.; Low, J.; Jiang, C.; Yu, J. Ultrathin 2d/2d wo3/g-c3n4 step-scheme h2-production photocatalyst. *Appl. Catal. B* **2019**, *243*, 556–565. [CrossRef]
70. Cao, A.; Zhang, L.; Wang, Y.; Zhao, H.; Deng, H.; Liu, X.; Lin, Z.; Su, X.; Yue, F. 2d–2d heterostructured unimof/g-c3n4 for enhanced photocatalytic h2 production under visible-light irradiation. *ACS Sustain. Chem. Eng.* **2019**, *7*, 2492–2499. [CrossRef]
71. Yuan, Y.-J.; Shen, Z.; Wu, S.; Su, Y.; Pei, L.; Ji, Z.; Ding, M.; Bai, W.; Chen, Y.; Yu, Z.-T.; et al. Liquid exfoliation of g-c3n4 nanosheets to construct 2d-2d mos2/g-C3N4 photocatalyst for enhanced photocatalytic h2 production activity. *Appl. Catal. B* **2019**, *246*, 120–128. [CrossRef]
72. Jiang, D.; Wen, B.; Zhang, Y.; Jin, Y.; Li, D.; Chen, M. Mos2/snnb2o6 2d/2d nanosheet heterojunctions with enhanced interfacial charge separation for boosting photocatalytic hydrogen evolution. *J. Colloid Interface Sci.* **2019**, *536*, 1–8. [CrossRef]
73. Gu, W.; Li, X.; Zhang, W.; Wang, J.; Yin, X.; Zhu, L.; Chen, Z.; Zou, W.; Fu, Z.; Lu, Y. Self-limited ion-exchange grown bi6fe2ti3o18-biobr ferroelectric heterostructure and the enhanced photocatalytic oxygen evolution. *Appl. Surf. Sci.* **2019**, *479*, 137–147. [CrossRef]
74. Ning, S.; Shi, X.; Zhang, H.; Lin, H.; Zhang, Z.; Long, J.; Li, Y.; Wang, X. Reconstructing dual-induced {0 0 1} facets bismuth oxychloride nanosheets heterostructures: An effective strategy to promote photocatalytic oxygen evolution. *Solar RRL* **2019**, *3*, 1900059. [CrossRef]
75. Sun, B.; Qian, Y.; Liang, Z.; Guo, Y.; Xue, Y.; Tian, J.; Cui, H. Oxygen vacancy-rich bio2-x ultra-thin nanosheet for efficient full-spectrum responsive photocatalytic oxygen evolution from water splitting. *Sol. Energy Mater. Sol. Cells* **2019**, *195*, 309–317. [CrossRef]
76. Li, L.; She, X.; Yi, J.; Pan, L.; Xia, K.; Wei, W.; Zhu, X.; Chen, Z.; Xu, H.; Li, H. Integrating coox cocatalyst on hexagonal α-fe2o3 for effective photocatalytic oxygen evolution. *Appl. Surf. Sci.* **2019**, *469*, 933–940. [CrossRef]
77. Tang, X.; Zhao, J.-H.; Li, Y.-H.; Zhou, Z.-J.; Li, K.; Liu, F.-T.; Lan, Y.-Q. Co-doped zn1−xcdxs nanocrystals from metal–organic framework precursors: Porous microstructure and efficient photocatalytic hydrogen evolution. *Dalton Trans.* **2017**, *46*, 10553–10557. [CrossRef]
78. Zhang, M.; Huang, Y.-L.; Wang, J.-W.; Lu, T.-B. A facile method for the synthesis of a porous cobalt oxide–carbon hybrid as a highly efficient water oxidation catalyst. *J. Mater. Chem. A* **2016**, *4*, 1819–1827. [CrossRef]
79. Jiang, L.; Yuan, X.; Pan, Y.; Liang, J.; Zeng, G.; Wu, Z.; Wang, H. Doping of graphitic carbon nitride for photocatalysis: A reveiw. *Appl. Catal. B* **2017**, *217*, 388–406. [CrossRef]
80. Masih, D.; Ma, Y.; Rohani, S. Graphitic c3n4 based noble-metal-free photocatalyst systems: A review. *Appl. Catal. B* **2017**, *206*, 556–588. [CrossRef]
81. Yang, X.; Chen, Z.; Xu, J.; Tang, H.; Chen, K.; Jiang, Y. Tuning the morphology of g-c3n4 for improvement of z-scheme photocatalytic water oxidation. *ACS Appl. Mater. Interfaces* **2015**, *7*, 15285–15293. [CrossRef]
82. Cao, S.; Yu, J. G-c3n4-based photocatalysts for hydrogen generation. *J. Phys. Chem. Lett.* **2014**, *5*, 2101–2107. [CrossRef]

83. Lam, S.-M.; Sin, J.-C.; Mohamed, A.R. A review on photocatalytic application of g-c3n4/semiconductor (cns) nanocomposites towards the erasure of dyeing wastewater. *Mater. Sci. Semicond. Process.* **2016**, *47*, 62–84. [CrossRef]
84. Hu, W.; Yuan, X.; Liu, X.; Guan, Y.; Wu, X. Hierarchical sno_2 nanostructures as high efficient photocatalysts for the degradation of organic dyes. *J. Sol-Gel Sci. Technol.* **2017**, *84*, 316–322. [CrossRef]
85. Gu, Q.; Gao, Z.; Zhao, H.; Lou, Z.; Liao, Y.; Xue, C. Temperature-controlled morphology evolution of graphitic carbon nitride nanostructures and their photocatalytic activities under visible light. *RSC Adv.* **2015**, *5*, 49317–49325. [CrossRef]
86. Lan, Z.-A.; Zhang, G.; Wang, X. A facile synthesis of br-modified g-c3n4 semiconductors for photoredox water splitting. *Appl. Catal. B* **2016**, *192*, 116–125. [CrossRef]
87. Yan, J.; Wu, H.; Chen, H.; Zhang, Y.; Zhang, F.; Liu, S.F. Fabrication of tio2/c3n4 heterostructure for enhanced photocatalytic z-scheme overall water splitting. *Appl. Catal. B* **2016**, *191*, 130–137. [CrossRef]
88. Zhou, H.; Hu, L.; Wan, J.; Yang, R.; Yu, X.; Li, H.; Chen, J.; Wang, L.; Lu, X. Microwave-enhanced catalytic degradation of p-nitrophenol in soil using mgfe2o4. *Chem. Eng. J.* **2016**, *284*, 54–60. [CrossRef]
89. Yang, Y.; Li, X.; Lu, C.; Huang, W. G-c3n4 nanosheets coupled with tio2 nanosheets as 2d/2d heterojunction photocatalysts toward high photocatalytic activity for hydrogen production. *Catal. Lett.* **2019**, *149*, 2930–2939. [CrossRef]
90. Zeng, Y.; Wang, Y.; Chen, J.; Jiang, Y.; Kiani, M.; Li, B.; Wang, R. Fabrication of high-activity hybrid nitio3/g-c3n4 heterostructured photocatalysts for water splitting to enhanced hydrogen production. *Ceram. Int.* **2016**, *42*, 12297–12305. [CrossRef]
91. She, X.; Liu, L.; Ji, H.; Mo, Z.; Li, Y.; Huang, L.; Du, D.; Xu, H.; Li, H. Template-free synthesis of 2d porous ultrathin nonmetal-doped g-c3n4 nanosheets with highly efficient photocatalytic h2 evolution from water under visible light. *Appl. Catal. B* **2016**, *187*, 144–153. [CrossRef]
92. Kadi, M.W.; Mohamed, R.M. Increasing visible light water splitting efficiency through synthesis route and charge separation in measoporous g-c3n4 decorated with wo3 nanoparticles. *Ceram. Int.* **2019**, *45*, 3886–3893. [CrossRef]
93. Xu, D.; Li, L.; Xia, T.; Fan, W.; Wang, F.; Bai, H.; Shi, W. Heterojunction composites of g-c3n4/knbo3 enhanced photocatalytic properties for water splitting. *Int. J. Hydrogen Energy* **2018**, *43*, 16566–16572. [CrossRef]
94. Seza, A.; Soleimani, F.; Naseri, N.; Soltaninejad, M.; Montazeri, S.; Sadrnezhaad, S.; Mohammadi, M.; Moghadam, H.A.; Forouzandeh, M.; Amin, M. Novel microwave-assisted synthesis of porous g-c3n4/sno2 nanocomposite for solar water-splitting. *Appl. Surf. Sci.* **2018**, *440*, 153–161. [CrossRef]
95. Xiao, J.; Zhang, X.; Li, Y. A ternary g-c3n4/pt/zno photoanode for efficient photoelectrochemical water splitting. *Int. J. Hydrogen Energy* **2015**, *40*, 9080–9087. [CrossRef]
96. Guo, F.; Shi, W.; Zhu, C.; Li, H.; Kang, Z. Coo and g-c3n4 complement each other for highly efficient overall water splitting under visible light. *Appl. Catal. B* **2018**, *226*, 412–420. [CrossRef]
97. He, K.; Xie, J.; Liu, Z.-Q.; Li, N.; Chen, X.; Hu, J.; Li, X. Multi-functional ni3c cocatalyst/g-c3n4 nanoheterojunctions for robust photocatalytic h2 evolution under visible light. *J. Mater. Chem. A* **2018**, *6*, 13110–13122. [CrossRef]
98. Chen, L.; Huang, H.; Zheng, Y.; Sun, W.; Zhao, Y.; Francis, P.S.; Wang, X. Noble-metal-free ni3n/g-c3n4 photocatalysts with enhanced hydrogen production under visible light irradiation. *Dalton Trans.* **2018**, *47*, 12188–12196. [CrossRef]
99. Chen, S.-H.; Wang, J.-J.; Huang, J.; Li, Q.-X. G-c3n4/sns2 heterostructure: A promising water splitting photocatalyst. *Chin. J. Chem. Phys.* **2017**, *30*, 36–42. [CrossRef]
100. Shen, R.; Xie, J.; Zhang, H.; Zhang, A.; Chen, X.; Li, X. Enhanced solar fuel h2 generation over g-c3n4 nanosheet photocatalysts by the synergetic effect of noble metal-free co2p cocatalyst and the environmental phosphorylation strategy. *ACS Sustain. Chem. Eng.* **2018**, *6*, 816–826. [CrossRef]
101. Sun, X.-J.; Yang, D.-D.; Dong, H.; Meng, X.-B.; Sheng, J.-L.; Zhang, X.; Wei, J.-Z.; Zhang, F.-M. Zif-derived cop as a cocatalyst for enhanced photocatalytic h2 production activity of g-c3n4. *Sustain. Energy Fuels* **2018**, *2*, 1356–1361. [CrossRef]
102. Wang, Y.; Liu, X.; Liu, J.; Han, B.; Hu, X.; Yang, F.; Xu, Z.; Li, Y.; Jia, S.; Li, Z.; et al. Carbon quantum dot implanted graphite carbon nitride nanotubes: Excellent charge separation and enhanced photocatalytic hydrogen evolution. *Angew. Chem.* **2018**, *57*, 5765–5771. [CrossRef]

103. Wang, N.; Li, J.; Wu, L.; Li, X.; Shu, J. Mno2 and carbon nanotube co-modified c3n4 composite catalyst for enhanced water splitting activity under visible light irradiation. *Int. J. Hydrogen Energy* **2016**, *41*, 22743–22750. [CrossRef]
104. Wang, M.; Ju, P.; Li, J.; Zhao, Y.; Han, X.; Hao, Z. Facile synthesis of mos2/g-c3n4/go ternary heterojunction with enhanced photocatalytic activity for water splitting. *ACS Sustain. Chem. Eng.* **2017**, *5*, 7878–7886. [CrossRef]
105. Schedin, F.; Geim, A.; Morozov, S.; Hill, E.; Blake, P.; Katsnelson, M.; Novoselov, K. Detection of individual gas molecules adsorbed on graphene. *Nat. Mater.* **2007**, *6*, 652. [CrossRef] [PubMed]
106. Warner, J.H.; Schäffel, F.; Bachmatiuk, A.; Rümmeli, M.H. (Eds.) Chapter 3—Properties of graphene. In *Graphene, Warner*; Woodhead Publishing: Cambridge, UK, 2013; pp. 61–127.
107. Choi, W.; Lahiri, I.; Seelaboyina, R.; Kang, Y.S. Synthesis of graphene and its applications: A review. *Crit. Rev. Solid State Mater. Sci.* **2010**, *35*, 52–71. [CrossRef]
108. Montes-Navajas, P.; Asenjo, N.G.; Santamaria, R.; Menendez, R.; Corma, A.; Garcia, H. Surface area measurement of graphene oxide in aqueous solutions. *Langmuir ACS J. Surf. Colloids* **2013**, *29*, 13443–13448. [CrossRef]
109. Lv, X.-J.; Zhou, S.-X.; Zhang, C.; Chang, H.-X.; Chen, Y.; Fu, W.-F. Synergetic effect of cu and graphene as cocatalyst on tio 2 for enhanced photocatalytic hydrogen evolution from solar water splitting. *J. Mater. Chem.* **2012**, *22*, 18542–18549. [CrossRef]
110. Giovannetti, R.; Rommozzi, E.; Zannotti, M.; D'Amato, C.A. Recent advances in graphene based tio2 nanocomposites (gtio2ns) for photocatalytic degradation of synthetic dyes. *Catalysts* **2017**, *7*, 305. [CrossRef]
111. Yan, Y.; Chen, J.; Li, N.; Tian, J.; Li, K.; Jiang, J.; Liu, J.; Tian, Q.; Chen, P. Systematic bandgap engineering of graphene quantum dots and applications for photocatalytic water splitting and co2 reduction. *ACS Nano* **2018**, *12*, 3523–3532. [CrossRef]
112. Del Pino, A.P.; González-Campo, A.; Giraldo, S.; Peral, J.; György, E.; Logofatu, C.; Puigmartí-Luis, J. Synthesis of graphene-based photocatalysts for water splitting by laser-induced doping with ionic liquids. *Carbon* **2018**, *130*, 48–58. [CrossRef]
113. Min, S.; Wang, F.; Lu, G. Graphene-induced spatial charge separation for selective water splitting over tio2 photocatalyst. *Catal. Commun.* **2016**, *80*, 28–32. [CrossRef]
114. Bellamkonda, S.; Thangavel, N.; Hafeez, H.Y.; Neppolian, B.; Rao, G.R. Highly active and stable multi-walled carbon nanotubes-graphene-tio2 nanohybrid: An efficient non-noble metal photocatalyst for water splitting. *Catal. Today* **2019**, *321*, 120–127. [CrossRef]
115. Mateo, D.; Esteve-Adell, I.; Albero, J.; Royo, J.F.S.; Primo, A.; Garcia, H. 111 oriented gold nanoplatelets on multilayer graphene as visible light photocatalyst for overall water splitting. *Nat. Commun.* **2016**, *7*, 11819. [CrossRef] [PubMed]
116. Mohamed, M.M.; Ibrahim, I.; Salama, T.M. Rational design of manganese ferrite-graphene hybrid photocatalysts: Efficient water splitting and effective elimination of organic pollutants. *Appl. Catal. A* **2016**, *524*, 182–191. [CrossRef]
117. Iwashina, K.; Iwase, A.; Ng, Y.H.; Amal, R.; Kudo, A. Z-schematic water splitting into h2 and o2 using metal sulfide as a hydrogen-evolving photocatalyst and reduced graphene oxide as a solid-state electron mediator. *J. Am. Chem. Soc.* **2015**, *137*, 604–607. [CrossRef] [PubMed]
118. Pan, Z.; Hisatomi, T.; Wang, Q.; Chen, S.; Iwase, A.; Nakabayashi, M.; Shibata, N.; Takata, T.; Katayama, M.; Minegishi, T. Photoreduced graphene oxide as a conductive binder to improve the water splitting activity of photocatalyst sheets. *Adv. Funct. Mater.* **2016**, *26*, 7011–7019. [CrossRef]
119. Shudo, Y.; Karim, M.R.; Wakata, K.; Ohmagari, H.; Kameda, N.; Hayami, S. Reduced graphene oxide-transition metal hybrids for hydrogen generation by photocatalytic water splitting. *J. Incl. Phenom. Macrocycl. Chem.* **2018**, 1–4. [CrossRef]
120. Fan, X.; Peng, Z.; Ye, R.; Zhou, H.; Guo, X. M3c (m: Fe, co, ni) nanocrystals encased in graphene nanoribbons: An active and stable bifunctional electrocatalyst for oxygen reduction and hydrogen evolution reactions. *ACS Nano* **2015**, *9*, 7407–7418. [CrossRef]
121. Jing, Y.; Tang, Q.; He, P.; Zhou, Z.; Shen, P. Small molecules make big differences: Molecular doping effects on electronic and optical properties of phosphorene. *Nanotechnology* **2015**, *26*, 095201. [CrossRef]
122. Khandelwal, A.; Mani, K.; Karigerasi, M.H.; Lahiri, I. Phosphorene–the two-dimensional black phosphorous: Properties, synthesis and applications. *Mater. Sci. Eng. B* **2017**, *221*, 17–34. [CrossRef]

123. Churchill, H.O.; Jarillo-Herrero, P. Two-dimensional crystals: Phosphorus joins the family. *Nat. Nanotechnol.* **2014**, *9*, 330. [CrossRef]
124. Lee, T.H.; Kim, S.Y.; Jang, H.W. Black phosphorus: Critical review and potential for water splitting photocatalyst. *Nanomaterials* **2016**, *6*, 194. [CrossRef]
125. Hu, J.; Chen, D.; Mo, Z.; Li, N.; Xu, Q.; Li, H.; He, J.; Xu, H.; Lu, J. Z-scheme 2d/2d heterojunction of black phosphorus/monolayer bi2wo6 nanosheets with enhanced photocatalytic activities. *Angew. Chem. Int. Ed.* **2019**, *58*, 2073–2077. [CrossRef] [PubMed]
126. Kou, L.; Chen, C.; Smith, S.C. Phosphorene: Fabrication, properties, and applications. *J. Phys. Chem. Lett.* **2015**, *6*, 2794–2805. [CrossRef] [PubMed]
127. Lee, H.U.; Lee, S.C.; Won, J.; Son, B.-C.; Choi, S.; Kim, Y.; Park, S.Y.; Kim, H.-S.; Lee, Y.-C.; Lee, J. Stable semiconductor black phosphorus (bp)@ titanium dioxide (tio 2) hybrid photocatalysts. *Sci. Rep.* **2015**, *5*, 8691. [CrossRef] [PubMed]
128. Cai, Y.; Zhang, G.; Zhang, Y.-W. Electronic properties of phosphorene/graphene and phosphorene/hexagonal boron nitride heterostructures. *J. Phys. Chem. C* **2015**, *119*, 13929–13936. [CrossRef]
129. Tian, B.; Tian, B.; Smith, B.; Scott, M.C.; Hua, R.; Lei, Q.; Tian, Y. Supported black phosphorus nanosheets as hydrogen-evolving photocatalyst achieving 5.4% energy conversion efficiency at 353 k. *Nat. Commun.* **2018**, *9*, 1397. [CrossRef]
130. Guo, H.; Lu, N.; Dai, J.; Wu, X.; Zeng, X.C. Phosphorene nanoribbons, phosphorus nanotubes, and van der waals multilayers. *J. Phys. Chem. C* **2014**, *118*, 14051–14059. [CrossRef]
131. Huang, L.; Huo, N.; Li, Y.; Chen, H.; Yang, J.; Wei, Z.; Li, J.; Li, S.-S. Electric-field tunable band offsets in black phosphorus and mos2 van der waals pn heterostructure. *J. Phys. Chem. Lett.* **2015**, *6*, 2483–2488. [CrossRef]
132. Yuan, Y.-P.; Ruan, L.-W.; Barber, J.; Loo, S.C.J.; Xue, C. Hetero-nanostructured suspended photocatalysts for solar-to-fuel conversion. *Energy Environ. Sci.* **2014**, *7*, 3934–3951. [CrossRef]
133. Shi, Y.; Zhang, B. Recent advances in transition metal phosphide nanomaterials: Synthesis and applications in hydrogen evolution reaction. *Chem. Soc. Rev.* **2016**, *45*, 1529–1541. [CrossRef]
134. Pan, Y.; Liu, Y.; Zhao, J.; Yang, K.; Liang, J.; Liu, D.; Hu, W.; Liu, D.; Liu, Y.; Liu, C. Monodispersed nickel phosphide nanocrystals with different phases: Synthesis, characterization and electrocatalytic properties for hydrogen evolution. *J. Mater. Chem. A* **2015**, *3*, 1656–1665. [CrossRef]
135. Anantharaj, S.; Ede, S.R.; Sakthikumar, K.; Karthick, K.; Mishra, S.; Kundu, S. Recent trends and perspectives in electrochemical water splitting with an emphasis on sulfide, selenide, and phosphide catalysts of fe, co, and ni: A review. *ACS Catal.* **2016**, *6*, 8069–8097. [CrossRef]
136. Ledendecker, M.; Krick Calderón, S.; Papp, C.; Steinrück, H.-P.; Antonietti, M.; Shalom, M. The synthesis of nanostructured ni5p4 films and their use as a non-noble bifunctional electrocatalyst for full water splitting. *Angew. Chem. Int. Ed.* **2015**, *54*, 12361–12365. [CrossRef] [PubMed]
137. Stern, L.-A.; Feng, L.; Song, F.; Hu, X. Ni2p as a janus catalyst for water splitting: The oxygen evolution activity of ni2p nanoparticles. *Energy Environ. Sci.* **2015**, *8*, 2347–2351. [CrossRef]
138. Yang, Y.; Fei, H.; Ruan, G.; Tour, J.M. Porous cobalt-based thin film as a bifunctional catalyst for hydrogen generation and oxygen generation. *Adv. Mater.* **2015**, *27*, 3175–3180. [CrossRef] [PubMed]
139. Sumboja, A.; An, T.; Goh, H.Y.; Lubke, M.; Howard, D.P.; Xu, Y.; Handoko, A.D.; Zong, Y.; Liu, Z. One-step facile synthesis of cobalt phosphides for hydrogen evolution reaction catalysts in acidic and alkaline medium. *ACS Appl. Mater. Interfaces* **2018**, *10*, 15673–15680. [CrossRef] [PubMed]
140. Su, L.; Cui, X.; He, T.; Zeng, L.; Tian, H.; Song, Y.; Qi, K.; Xia, B.Y. Surface reconstruction of cobalt phosphide nanosheets by electrochemical activation for enhanced hydrogen evolution in alkaline solution. *Chem. Sci.* **2019**, *10*, 2019–2024. [CrossRef]
141. Zhu, Y.-P.; Liu, Y.-P.; Ren, T.-Z.; Yuan, Z.-Y. Self-supported cobalt phosphide mesoporous nanorod arrays: A flexible and bifunctional electrode for highly active electrocatalytic water reduction and oxidation. *Adv. Funct. Mater.* **2015**, *25*, 7337–7347. [CrossRef]
142. Li, Y.; Zhang, H.; Jiang, M.; Kuang, Y.; Sun, X.; Duan, X. Ternary nicop nanosheet arrays: An excellent bifunctional catalyst for alkaline overall water splitting. *Nano Res.* **2016**, *9*, 2251–2259. [CrossRef]
143. Liang, H.; Gandi, A.N.; Anjum, D.H.; Wang, X.; Schwingenschlogl, U.; Alshareef, H.N. Plasma-assisted synthesis of nicop for efficient overall water splitting. *Nano Lett.* **2016**, *16*, 7718–7725. [CrossRef]

144. Wu, R.; Xiao, B.; Gao, Q.; Zheng, Y.-R.; Zheng, X.-S.; Zhu, J.-F.; Gao, M.-R.; Yu, S.-H. A janus nickel cobalt phosphide catalyst for high-efficiency neutral-ph water splitting. *Angew. Chem. Int. Ed.* **2018**, *57*, 15445–15449. [CrossRef]
145. Du, C.; Yang, L.; Yang, F.; Cheng, G.; Luo, W. Nest-like nicop for highly efficient overall water splitting. *ACS Catal.* **2017**, *7*, 4131–4137. [CrossRef]
146. Orlandi, M.; Brenna, D.; Harms, R.; Jost, S.; Benaglia, M. Recent developments in the reduction of aromatic and aliphatic nitro compounds to amines. *Org. Process Res. Dev.* **2016**, *22*, 430–445. [CrossRef]
147. Ma, X.; Chang, Y.; Zhang, Z.; Tang, J. Forest-like nicop@cu3p supported on copper foam as a bifunctional catalyst for efficient water splitting. *J. Mater. Chem. A* **2018**, *6*, 2100–2106. [CrossRef]
148. Tong, M.; Wang, L.; Yu, P.; Liu, X.; Fu, H. 3d network nanostructured nicop nanosheets supported on n-doped carbon coated ni foam as a highly active bifunctional electrocatalyst for hydrogen and oxygen evolution reactions. *Front. Chem. Sci. Eng.* **2018**, *12*, 417–424. [CrossRef]
149. Du, D.Y.; Qin, J.S.; Li, S.L.; Su, Z.M.; Lan, Y.Q. Recent advances in porous polyoxometalate-based metal-organic framework materials. *Chem. Soc. Rev.* **2014**, *43*, 4615–4632. [CrossRef] [PubMed]
150. Bordiga, S.; Lamberti, C.; Ricchiardi, G.; Regli, L.; Bonino, F.; Damin, A.; Lillerud, K.P.; Bjorgen, M.; Zecchina, A. Electronic and vibrational properties of a mof-5 metal-organic framework: Zno quantum dot behaviour. *Chem. Commun. (Camb. Engl.)* **2004**, 2300–2301. [CrossRef]
151. Tachikawa, T.; Choi, J.R.; Fujitsuka, M.; Majima, T. Photoinduced charge-transfer processes on mof-5 nanoparticles: Elucidating differences between metal-organic frameworks and semiconductor metal oxides. *J. Phys. Chem. C* **2008**, *112*, 14090–14101. [CrossRef]
152. Bauer, C.A.; Timofeeva, T.V.; Settersten, T.B.; Patterson, B.D.; Liu, V.H.; Simmons, B.A.; Allendorf, M.D. Influence of connectivity and porosity on ligand-based luminescence in zinc metal-organic frameworks. *J. Am. Chem. Soc.* **2007**, *129*, 7136–7144. [CrossRef]
153. Li, F.; Jiang, X.; Zhao, J.; Zhang, S. Graphene oxide: A promising nanomaterial for energy and environmental applications. *Nano Energy* **2015**, *16*, 488–515. [CrossRef]
154. Zhang, X.; Liu, S.; Zang, Y.; Liu, R.; Liu, G.; Wang, G.; Zhang, Y.; Zhang, H.; Zhao, H. Co/co 9 s 8 @s,n-doped porous graphene sheets derived from s, n dual organic ligands assembled co-mofs as superior electrocatalysts for full water splitting in alkaline media. *Nano Energy* **2016**, *30*, 93–102. [CrossRef]
155. Xiao, J.-D.; Shang, Q.; Xiong, Y.; Zhang, Q.; Luo, Y.; Yu, S.-H.; Jiang, H.-L. Boosting photocatalytic hydrogen production of a metal–organic framework decorated with platinum nanoparticles: The platinum location matters. *Angew. Chem.* **2016**, *128*, 9535–9539. [CrossRef]
156. Qin, J.S.; Zhang, S.R.; Du, D.Y.; Shen, P.; Bao, S.J.; Lan, Y.Q.; Su, Z.M. A microporous anionic metal-organic framework for sensing luminescence of lanthanide(iii) ions and selective absorption of dyes by ionic exchange. *Chemistry* **2014**, *20*, 5625–5630. [CrossRef] [PubMed]
157. Gao, C.Y.; Tian, H.R.; Ai, J.; Li, L.J.; Dang, S.; Lan, Y.Q.; Sun, Z.M. A microporous cu-mof with optimized open metal sites and pore spaces for high gas storage and active chemical fixation of co2. *Chem. Commun. (Camb. Engl.)* **2016**, *52*, 11147–11150. [CrossRef] [PubMed]
158. Gascon, J.; Corma, A.; Kapteijn, F.; Llabrés i Xamena, F.X. Metal organic framework catalysis: Quo vadis? *ACS Catal.* **2014**, *4*, 361–378. [CrossRef]
159. Wang, C.; Liu, D.; Lin, W. Metal-organic frameworks as a tunable platform for designing functional molecular materials. *J. Am. Chem. Soc.* **2013**, *135*, 13222–13234. [CrossRef]
160. Zhang, T.; Lin, W. Metal-organic frameworks for artificial photosynthesis and photocatalysis. *Chem. Soc. Rev.* **2014**, *43*, 5982–5993. [CrossRef]
161. Song, F.; Li, W.; Sun, Y. Metal–organic frameworks and their derivatives for photocatalytic water splitting. *Inorganics* **2017**, *5*, 40. [CrossRef]
162. Wang, W.; Xu, X.; Zhou, W.; Shao, Z. Recent progress in metal-organic frameworks for applications in electrocatalytic and photocatalytic water splitting. *Adv. Sci.* **2017**, *4*, 1600371. [CrossRef]
163. Long, J.; Wang, S.; Ding, Z.; Wang, S.; Zhou, Y.; Huang, L.; Wang, X. Amine-functionalized zirconium metal-organic framework as efficient visible-light photocatalyst for aerobic organic transformations. *Chem. Commun. (Camb. Engl.)* **2012**, *48*, 11656–11658. [CrossRef]
164. Horiuchi, Y.; Toyao, T.; Saito, M.; Mochizuki, K.; Iwata, M.; Higashimura, H.; Anpo, M.; Matsuoka, M. Visible-light-promoted photocatalytic hydrogen production by using an amino-functionalized ti(iv) metal–organic framework. *J. Phys. Chem. C* **2012**, *116*, 20848–20853. [CrossRef]

165. Fateeva, A.; Chater, P.A.; Ireland, C.P.; Tahir, A.A.; Khimyak, Y.Z.; Wiper, P.V.; Darwent, J.R.; Rosseinsky, M.J. A water-stable porphyrin-based metal-organic framework active for visible-light photocatalysis. *Angew. Chem.* **2012**, *51*, 7440–7444. [CrossRef] [PubMed]
166. Wang, C.; Xie, Z.; deKrafft, K.E.; Lin, W. Doping metal-organic frameworks for water oxidation, carbon dioxide reduction, and organic photocatalysis. *J. Am. Chem. Soc.* **2011**, *133*, 13445–13454. [CrossRef] [PubMed]
167. Xiang, W.; Zhang, Y.; Lin, H.; Liu, C.J. Nanoparticle/metal-organic framework composites for catalytic applications: Current status and perspective. *Molecules* **2017**, *22*, 2103. [CrossRef] [PubMed]
168. Bala, S.; Mondal, I.; Goswami, A.; Pal, U.; Mondal, R. Co-mof as a sacrificial template: Manifesting a new co3o4/tio2 system with a p–n heterojunction for photocatalytic hydrogen evolution. *J. Mater. Chem. A* **2015**, *3*, 20288–20296. [CrossRef]
169. Lan, M.; Guo, R.-M.; Dou, Y.; Zhou, J.; Zhou, A.; Li, J.-R. Fabrication of porous pt-doping heterojunctions by using bimetallic mof template for photocatalytic hydrogen generation. *Nano Energy* **2017**, *33*, 238–246. [CrossRef]
170. Jiang, Z.; Lu, W.; Li, Z.; Ho, K.H.; Li, X.; Jiao, X.; Chen, D. Synthesis of amorphous cobalt sulfide polyhedral nanocages for high performance supercapacitors. *J. Mater. Chem. A* **2014**, *2*, 8603–8606. [CrossRef]
171. Venna, S.R.; Jasinski, J.B.; Carreon, M.A. Structural evolution of zeolitic imidazolate framework-8. *J. Am. Chem. Soc.* **2010**, *132*, 18030–18033. [CrossRef]
172. Yu, B.; Zhang, D.; Du, S.; Wang, Y.; Chen, M.; Hou, J.; Xu, S.; Wu, S.; Gong, J. Phase transfer directed synthesis of hollow zeolitic imidazolate frameworks-67 nanocages. *Cryst. Growth Des.* **2016**, *17*, 3–6. [CrossRef]
173. Xu, W.; Li, T.-T.; Zheng, Y.-Q. Porous co3o4 nanoparticles derived from a co(ii)-cyclohexanehexacarboxylate metal–organic framework and used in a supercapacitor with good cycling stability. *RSC Adv.* **2016**, *6*, 86447–86454. [CrossRef]
174. Wang, C.; deKrafft, K.E.; Lin, W. Pt nanoparticles@photoactive metal–organic frameworks: Efficient hydrogen evolution via synergistic photoexcitation and electron injection. *J. Am. Chem. Soc.* **2012**, *134*, 7211–7214. [CrossRef]
175. Wang, D.; Song, Y.; Cai, J.; Wu, L.; Li, Z. Effective photo-reduction to deposit pt nanoparticles on mil-100(fe) for visible-light-induced hydrogen evolution. *New J. Chem.* **2016**, *40*, 9170–9175. [CrossRef]
176. Laurier, K.G.; Vermoortele, F.; Ameloot, R.; De Vos, D.E.; Hofkens, J.; Roeffaers, M.B. Iron(iii)-based metal-organic frameworks as visible light photocatalysts. *J. Am. Chem. Soc.* **2013**, *135*, 14488–14491. [CrossRef]
177. Liu, Q.; Xie, L.; Shi, X.; Du, G.; Asiri, A.M.; Luo, Y.; Sun, X. High-performance water oxidation electrocatalysis enabled by a ni-mof nanosheet array. *Inorg. Chem. Front.* **2018**, *5*, 1570–1574. [CrossRef]
178. Zhao, S.; Wang, Y.; Dong, J.; He, C.-T.; Yin, H.; An, P.; Zhao, K.; Zhang, X.; Gao, C.; Zhang, L.; et al. Ultrathin metal–organic framework nanosheets for electrocatalytic oxygen evolution. *Nat. Energy* **2016**, *1*, 16184. [CrossRef]
179. Duan, J.; Chen, S.; Zhao, C. Ultrathin metal-organic framework array for efficient electrocatalytic water splitting. *Nat. Commun.* **2017**, *8*, 15341. [CrossRef]
180. Lin, R.; Shen, L.; Ren, Z.; Wu, W.; Tan, Y.; Fu, H.; Zhang, J.; Wu, L. Enhanced photocatalytic hydrogen production activity via dual modification of mof and reduced graphene oxide on cds. *Chem. Commun.* **2014**, *50*, 8533–8535. [CrossRef]
181. Cavka, J.H.; Jakobsen, S.; Olsbye, U.; Guillou, N.; Lamberti, C.; Bordiga, S.; Lillerud, K.P. A new zirconium inorganic building brick forming metal organic frameworks with exceptional stability. *J. Am. Chem. Soc.* **2008**, *130*, 13850–13851. [CrossRef]
182. Gomes Silva, C.; Luz, I.; Llabres i Xamena, F.X.; Corma, A.; Garcia, H. Water stable zr-benzenedicarboxylate metal-organic frameworks as photocatalysts for hydrogen generation. *Chemistry* **2010**, *16*, 11133–11138. [CrossRef]
183. Shen, L.; Luo, M.; Liu, Y.; Liang, R.; Jing, F.; Wu, L. Noble-metal-free mos2 co-catalyst decorated uio-66/cds hybrids for efficient photocatalytic h2 production. *Appl. Catal. B* **2015**, *166–167*, 445–453. [CrossRef]
184. He, J.; Yan, Z.; Wang, J.; Xie, J.; Jiang, L.; Shi, Y.; Yuan, F.; Yu, F.; Sun, Y. Significantly enhanced photocatalytic hydrogen evolution under visible light over cds embedded on metal–organic frameworks. *Chem. Commun.* **2013**, *49*, 6761–6763. [CrossRef]

185. Wen, M.; Mori, K.; Kamegawa, T.; Yamashita, H. Amine-functionalized mil-101(cr) with imbedded platinum nanoparticles as a durable photocatalyst for hydrogen production from water. *Chem. Commun.* **2014**, *50*, 11645–11648. [CrossRef]
186. Han, J.; Wang, D.; Du, Y.; Xi, S.; Hong, J.; Yin, S.; Chen, Z.; Zhou, T.; Xu, R. Metal–organic framework immobilized cobalt oxide nanoparticles for efficient photocatalytic water oxidation. *J. Mater. Chem. A* **2015**, *3*, 20607–20613. [CrossRef]
187. Sun, X.; Yu, Q.; Zhang, F.; Wei, J.; Yang, P. A dye-like ligand-based metal–organic framework for efficient photocatalytic hydrogen production from aqueous solution. *Catal. Sci. Technol.* **2016**, *6*, 3840–3844. [CrossRef]
188. Yang, D.; Sun, Y.; Tong, Z.; Tian, Y.; Li, Y.; Jiang, Z. Synthesis of ag/tio2 nanotube heterojunction with improved visible-light photocatalytic performance inspired by bioadhesion. *J. Phys. Chem. C* **2015**, *119*, 5827–5835. [CrossRef]
189. He, J.; Wang, J.; Chen, Y.; Zhang, J.; Duan, D.; Wang, Y.; Yan, Z. A dye-sensitized pt@uio-66(zr) metal-organic framework for visible-light photocatalytic hydrogen production. *Chem. Commun. (Camb. Engl.)* **2014**, *50*, 7063–7066. [CrossRef]
190. Nguyen, T.N.; Kampouri, S.; Valizadeh, B.; Luo, W.; Ongari, D.; Planes, O.M.; Zuttel, A.; Smit, B.; Stylianou, K.C. Photocatalytic hydrogen generation from a visible-light-responsive metal-organic framework system: Stability versus activity of molybdenum sulfide cocatalysts. *ACS Appl. Mater. Interfaces* **2018**, *10*, 30035–30039. [CrossRef]
191. Rao, C.N.R.; Maitra, U.; Waghmare, U.V. Extraordinary attributes of 2-dimensional mos2 nanosheets. *Chem. Phys. Lett.* **2014**, *609*, 172–183. [CrossRef]
192. Jaramillo, T.F.; Jorgensen, K.P.; Bonde, J.; Nielsen, J.H.; Horch, S.; Chorkendorff, I. Identification of active edge sites for electrochemical h2 evolution from mos2 nanocatalysts. *Science (N. Y.)* **2007**, *317*, 100–102. [CrossRef]
193. Ataca, C.; Ciraci, S. Dissociation of h2o at the vacancies of single-layer mos2. *Biophys. Rev. B* **2012**, *85*, 195410. [CrossRef]
194. Laursen, A.B.; Kegnæs, S.; Dahl, S.; Chorkendorff, I. Molybdenum sulfides—efficient and viable materials for electro - and photoelectrocatalytic hydrogen evolution. *Energy Environ. Sci.* **2012**, *5*, 5577. [CrossRef]
195. Van Gastel, M.; Shaw, J.L.; Blake, A.J.; Flores, M.; Schröder, M.; McMaster, J.; Lubitz, W. Electronic structure of a binuclear nickel complex of relevance to [nife] hydrogenase. *Inorg. Chem.* **2008**, *47*, 11688–11697. [CrossRef]
196. Feng, Y.; Chen, C.; Liu, Z.; Fei, B.; Lin, P.; Li, Q.; Sun, S.; Du, S. Application of a ni mercaptopyrimidine mof as highly efficient catalyst for sunlight-driven hydrogen generation. *J. Mater. Chem. A* **2015**, *3*, 7163–7169. [CrossRef]
197. An, Y.; Liu, Y.; An, P.; Dong, J.; Xu, B.; Dai, Y.; Qin, X.; Zhang, X.; Whangbo, M.H.; Huang, B. Ni(ii) coordination to an al-based metal-organic framework made from 2-aminoterephthalate for photocatalytic overall water splitting. *Angew. Chem.* **2017**, *56*, 3036–3040. [CrossRef]
198. Zhou, T.; Du, Y.; Borgna, A.; Hong, J.; Wang, Y.; Han, J.; Zhang, W.; Xu, R. Post-synthesis modification of a metal–organic framework to construct a bifunctional photocatalyst for hydrogen production. *Energy Environ. Sci.* **2013**, *6*, 3229. [CrossRef]
199. Bloch, E.D.; Britt, D.; Lee, C.; Doonan, C.J.; Uribe-Romo, F.J.; Furukawa, H.; Long, J.R.; Yaghi, O.M. Metal insertion in a microporous metal-organic framework lined with 2,2′-bipyridine. *J. Am. Chem. Soc.* **2010**, *132*, 14382–14384. [CrossRef]
200. Toyao, T.; Saito, M.; Dohshi, S.; Mochizuki, K.; Iwata, M.; Higashimura, H.; Horiuchi, Y.; Matsuoka, M. Development of a ru complex-incorporated mof photocatalyst for hydrogen production under visible-light irradiation. *Chem. Commun. (Camb. Engl.)* **2014**, *50*, 6779–6781. [CrossRef]
201. Dhakshinamoorthy, A.; Asiri, A.M.; Garcia, H. 2d metal–organic frameworks as multifunctional materials in heterogeneous catalysis and electro/photocatalysis. *Adv. Mater.* **2019**, *31*, 1900617. [CrossRef]
202. Fajrina, N.; Tahir, M. A critical review in strategies to improve photocatalytic water splitting towards hydrogen production. *Int. J. Hydrogen Energy* **2019**, *44*, 540–577. [CrossRef]
203. Wang, Z.; Li, C.; Domen, K. Recent developments in heterogeneous photocatalysts for solar-driven overall water splitting. *Chem. Soc. Rev.* **2019**, *48*, 2109–2125. [CrossRef]